國 立 交 通 大 學

光電工程研究所

碩士論文

具有局部缺陷氮化鎵二維光子晶體面射型雷射光學特性之研究

GaN-based Photonic Crystal Surface Emitting Lasers with Localized Defects

研 究 生：侯 延 儒　　Student: Yen-Ju Hou

指導教授：盧 廷 昌　　Advisor: Tien-Chang Lu

郭 浩 中　　Hao-Chung Kuo

中華民國一百年一月

具有局部缺陷氮化鎵二維光子晶體面射型雷射光學特性之研究

GaN-based Photonic Crystal Surface Emitting Lasers with Localized Defects

研 究 生：侯延儒　　Student：Yen-Ju Hou

指導教授：盧廷昌　　Advisors：Tien-Chang Lu

郭浩中　　Hao-Chung Kuo

國 立 交 通 大 學

光 電 工 程 研 究 所

碩 士 論 文

A Thesis

Submitted to Institute of Electro-Optical Engineering

College of Electrical Engineering and Computer Science

National Chiao Tung University

in partial Fulfillment of the Requirements

for the Degree of Master

in

Electro-Optical Engineering

Jan 2011

Hsinchu, Taiwan, Republic of China

中 華 民 國 一 百 年 一 月

具有局部缺陷氮化鎵二維光子晶體面射型雷射光學特性之研究

研究生：侯延儒　　指導教授：盧廷昌 教授　郭浩中 教授

國立交通大學 光電工程研究所

摘 要

本篇論文研究具有局部缺陷氮化鎵二維光子晶體面射型雷射光學特性以及局部缺陷對雷射共振造成的影響。根據理論，在光子晶體周期結構中，雷射出射必須滿足布拉格繞射條件。因此，考慮樣品光致發光光譜中心波長400奈米，根據平面波展開法而設計光子晶體元件之晶格常數範圍190奈米。我們設計了四種不同的光子晶體元件，一種是沒有缺陷，而有缺陷的分為從中心到旁邊有三、四、五個週期光子晶體被挖空。沒有缺陷之光子晶體雷射發光波長為400奈米，隨著不同的缺陷大小，雷射波長以及雷射閾值會有所不同。為了了解其中變化的差異我們利用平面波展開法模擬光子晶體TE能帶圖。從實驗數據研究光子晶體雷射之正規化頻率正好相對於Γ1 之能帶邊界，表示雷射發生只在特定能帶邊界上。從極化狀態可證實雷射模態確實存在Γ1能帶邊緣。再來利用變角度解析螢光頻譜可以量測到對於不同缺陷之光子晶體雷射的E-K圖是類似的。於是我們利用共振腔之共振波長隨著腔長周期性變化的理論，算出對於不同缺陷大小之光子晶體雷射波長的變化。我們可以發現不同缺陷之光子晶體雷射分別對應到398奈米(H3) 392奈米(H4) 390奈米(H5)，是由於共振腔長之改變造成雷射波長的位移，而模擬的結果也和實驗吻合。此外，關於雷射閾值功率隨著缺陷變大而逐漸升高，是由於當光子晶體層數減少時，反射率以及共振之強度也隨之下降所造成之結果。

GaN-based Photonic Crystal Surface Emitting Lasers with Localized Defects

Student : Yen-Ju Hou **Advisor: Dr. T.C. Lu**

Dr. H.C. Kuo

Institute of electro-optical Engineering

National Chiao-Tung University

Abstract

In this thesis, we investigated the optical characteristics and the effect of defects in GaN-based 2D photonic crystal surface emitting lasers (PCSELs). According to the theory, the lasing behavior in the photonic crystal grating structure could only happen as the Bragg condition is satisfied. Therefore, the lattice constant is determined to be 190 nm considering PL peak of the samples centered at a wavelength of 400nm by the plane wave expansion theory. We designed four types of PCSELSs, one is without defect, the other is with there periods PC missing, the other is with four periods missing , another is with five periods missing .Lasing wavelengths and lasing threshold powers varies with different defect size. In order to realize the difference between these devices, we use plane wave expansion method (PWEM) to simulate the TE band diagram. Normalized frequency of investigated PC lasing wavelength can correspond to band-edge frequency (Γ1), which indicates the lasing action can only occur at specific band-edge mode. Polarization states further confirm the existence of lasing modes at band-edge (Γ1) mode. By the angle-resolved micro -photoluminescence measurement, we find out that the band structure of these band edge modes with or without defect are similar. Based on the cavity mode theory , cavity modes shifts with cavity length, we calculated cavity mode detuning with cavity lengths which indicates H3 corresponding to 398nm, H4 corresponding to 392 nm and H5 corresponding to 390 nm respectively. Besides, lasing threshold power increasing with larger defect size is the result of coupling and feedback strength decreasing with photonic crystal.

誌謝

從大三到現在踏入實驗室的生活，終於要在這階段告一段落了。直到現在，才有一點即將要畢業的感覺。這段日子裡所學到的東西太多了，不僅僅是學術研究上的知識，也包含了為人處事的態度，我要感謝那些在這幾年所有幫助我成長的人。在我遇到問題時不吝幫我解答，使我可以順利的完成我的碩士學位。

首先，我由衷的感謝王興宗老師的指導，老師做學問認真的態度深深地影響我，而在每次報告時老師的殷切叮嚀，我都有牢記在腦海裡。感謝盧廷昌老師的指導，使我能夠有許多想法去解決實驗上所遇到的問題。感謝郭浩中老師在我實驗上遭遇困難時，給予我幫助和鼓勵。

感謝宗鼎、士偉、板弟學長，平常Meeting上的指導以及對研究上的規劃和叮嚀，每當我開始怠惰，總是有學長在旁邊鞭策，以及研究上給予的幫助。感謝小馬學姐和阿綱學長，謝謝你在我碩一時教我熟習實驗的一切架構以及許多光子晶體的基礎知識；感謝翁翁、阿翔、依嚀、祥淇、永吉、惟雯、Joseph、阿飛、David、小昕、小胖等碩二的同學，因為你們而讓我的碩士生活更多采多姿。 還有感謝學弟幼齒、昀霖、思維、祐國在實驗和生活上的鼓勵和幫忙，希望你們實驗順利。

從大三專題到現在，感謝盧老師耐心的指導和鞭策，老師不厭其煩的帶著我看書、跑模擬 討論實驗的data等等，從以前懵懵懂懂對半導體發光材料一無所知的我，到現在的成長。

Contents

Figure Contents

Chapter 1

Introduction

1-1 Nitride-based materials

Nitride-based materials has been attracting much attentions during past decades, because of their large direct wide band-gap characteristics and can be widely used in various optoelectronic devices such as flat panel displays, optical storage, automobiles, illumination and so on[1-4]. These kind III-V wide band-gap materials implies large band off-set characteristic which can be utilized in hetero-structure and provides better carrier confinement. These kind materials band-gap diagram cover the range from sub-eV to several few eV. This is a promising potential for construct full-color display and solid-state lighting, including light emitting diodes (LEDs) and laser diodes (LDs). Furthermore, larger band-gap results in higher bulk material dielectric strength (higher voltage per unit thickness) and strong excitonic energy, which leads to more compact and higher frequency device. In addition, the peak drift velocity of electron in GaN can be double that of Si and GaAs (10^7 cm/s) at much higher electric fields. Also, semiconductor with large band-gap can operate in higher temperature. These characteristics results in the high efficiency GaN-based electro-optic device. However, the problem currently being addressed in GaN and AlN materials on large defect densities, piezoelectric field effect and spontaneous polarization. It appears that

growing defect-free GaN and AlN materials can be the limit to fabricate high quality and high power devices. Nowadays, there are many fundamental process breakthrough to tackle with how to control defects, threading dislocation, lattice mismatch in epitaxy. Therefore, the GaN-based materials with its superior properties make it a good candidate for the optoelectronic applications in next decades.

1-2 Photonic crystal in Nitride-Based materials

Photonic crystals, also known as photonic band gap structures, have been drawing much attention as new optical materials. The main feature of photonic crystals is that they have photonic band gaps for photons, which is similar to the electronic band structure for electrons in semiconductors. By utilizing the photonic band gaps and/or the dispersion relation between the photon energy and the wave vector, light emission and propagation can be controlled arbitrarily, and realization of various new optical devices and/or circuits is expected.

In nitride-based materials, photonic crystal is most widely used in light emitting diode (LED). In a usual LED, 90% of the light is trapped inside the structure due to the high refractive index of the material, mostly as guided modes[5]. To improve light extraction, photonic crystals(PhCs) [6] constitute a promising candidate, besides more classic approaches based on geometrical optics[7]. Several attempts have been made

to incorporate PhCs as “light extractors” notably for GaN materials[8]. In 2005, Nakamura *et al.* represented a method for observation of the band structure of a light-extracting photonic crystal in GaN, and bring evidence of its behavior as a true two-dimensional (2D) diffractive element in an overall three-dimensional (3D) structure[9]. They also pointed out that there are two main ways of improving light extraction by means of PhCs can be considered: one is the use of the PhCs band gaps to prevent emission in guided modes[10]; the other consists in using the PhCs to couple guided modes to radiative modes[11,12]. The first approach is challenging, due to the need to combine wavelength-sized microcavities with efficient electrical/optical injection and to the effect of nonradiative losses[13]. Hence, most of the extraction mechanism consider the second option, namely the use of a 2D PhCs to turn a guided mode (outside the PhCs) into a radiative pseudo-guided Bloch mode, lying above the light line of air.

1-3 Photonic Crystal Lasers

There are two types of photonic crystal lasers. The first type has a defect with optical gain surrounded by a PC mirror to form a resonant cavity and lasing actions arise from the defect. The second type of photonic crystal lasers, photonic crystal band edge laser, can operate without any defined cavity and extrinsic photonic crystal

mirror.

1-3.1 Photonic Crystal Nano Lasers

In 1994, P. R. Berman *et al.* first presented that photonic crystal could be a reflective mirror around the cavity of a laser [14]. Then, in 1999 O. Painter practically demonstrated an optically pumped InGaAs-based 2-D PC nano-cavity laser emitting 1.55 micrometers [15]. The optical cavity he demonstrated consisted of a half-wavelength-thick waveguide for vertical confinement and a 2-D PC mirror for lateral localization. A defect was introduced as a nano-cavity (a volume of 2.5 cubic half-wavelength, approximately 0.03 cubic micrometers) in the 2-D PC to trap photons inside. In 2004, Hong-Gyu Park *et al.* realized the electrically driven single-cell 2D-PC laser (λ=1519.7 nm) [16]. They used a sub-micrometer-sized semiconductor post placed at the center of the single-cell photonic crystal resonator to connect bottom electrode and achieved lasing action by current injection.

In 2005, nitride-based blue (about 488nm) photonic crystal membrane nano-cavity with Q factor about 800 was also reported by Y. S. Choi *et al.* [17]. They used photo-enhanced chemical etching to form a GaN membrane with a total thickness of 140 nm and patterned a photonic crystal cavity on it. Some resonance modes from the nano-cavities with lattice constant 180 nm could be observed in the photoluminescence (PL) emission.

1-3.2 Photonic Crystal Surface Emitting Lasers (PCSELs)

In 1946, Edward Purcell first proposed that spontaneous from excited states of an atom can be significantly altered by placing it in a low loss cavity with dimensions on the order of the electromagnetic wavelength [18]. Recently, with the advent of semiconductor laser and the improvement of crystal growth and fabrication, there has been increasing interest in engineering of optical micro-cavity in semiconductor for light emission control. Photonic crystal is a dielectric structure arranged in periodic geometry. Like a crystalline solid in electronic band structure. So photonic crystal can exhibit one or more photonic band gaps (PBGs), with frequency in band gap unable to propagate in the crystal. Photonic crystal with photonic band gaps for photons have many advantages in controlling the light emission, wave propagate along specific direction and can be utilized in many optoelectronic devices. For instance, photonic crystal passive waveguide used as low loss channel for light propagation and resonator to keep the whole cavity with high Q characteristic, which can be a promising device in conjunction with Si based and III-V materials communication system. Semiconductor with these unique properties can not only be used as a versatile building block to construct photonic circuitry but also an active medium to control light emission [19]. Two kinds of semiconductor photonic lasers have been demonstrated. One is 2D photonic crystal nano-cavity lasers, and the other is 2D

photonic crystal band-edge lasers.

According to the DFB theory, light at the photonic band-edge has zero group velocity and forms a standing wave due to 2D DFB effect. Specific band-edges induce not only in-plane coupling via DFB, but also diffraction normal to the PC plane, causing surface emission phenomena. In 1999, Noda *et al.* reported the electrically driven 2-D PC band-edge laser under pulsed operation [20]. The PC was a triangular-lattice structure composed of InP and air holes, which is integrated with an InGaAsP/InP multiple-quantum-well active layer by a wafer fusion technique. They demonstrated the single-mode, large-area and surface-emitting lasing action, and analyzed the lasing mechanism based on the satisfying of Bragg condition. Then, they further reported the room-temperature (RT) 2D PC band-edge laser under continuous wave (CW) operation in 2004 [21]. This opens a new road toward the large-area single-mode surface emitting laser.

1-4 Objective of the thesis

A considerable amount of literature has been published on photonic crystal surface emitting lasers utilizing a 2D distributed feedback (DFB) mechanism. Many works have been done about the lasing characteristics between different type of photonic crystal structures. In this thesis, we successfully fabricated different types of

localized defects in GaN-based 2D PCSELs and we focused on using Bragg theory and polarization to explain the lasing behavior. Finally we apply cavity mode detuning calculation to explain the difference between different types of defects in PCSELs. We would detail the whole story in the following sections.

1-5 Outline of the thesis

This thesis is organized in the following arrangement. The first chapter introduces the history of GaN materials and different types of photonic crystal lasers in GaN-based materials. Chapter 2 introduces the Bragg theory in 2D triangular lattice PhCs and cavity mode calculation in 1D approximation. Chapter 3 describes the wafer preparation and fabrication of PCSELs. Chapter 4 presents the experimental results analysis and simulations of defects in PCSELs. The last chapter assesses the conclusion and future work.

Reference

[1] S. Nakamura, M. Senoh, N. Iwasa, and S. Nagahama, *Jpn. J. Appl.Phys.*, **34**, L797 (1995)

[2] S. Nakamura, T. Mukai, and M. Senoh, *Appl. Phys. Lett.*,**64**, 1687 (1994)

[3] S. Nakamura, M. Senoh, S.Nagahama, N.Iwasa, T. Yamada, T. Matsushita, Y. Sugimoto, and H.Kiyoku, *Appl. Phys. Lett.*, **70**, 868 (1997)

[4] S. Nakamura, *Science*, **281**, 956 (1998)

[5] H. Benisty, H. De Neve, and C. Weisbuch, *IEEE J. Quantum Electron.* **34**, 1612 (1998); **34**, 1632 (1998).

[6] E. Yablonovitch, *Phys. Rev. Lett.* **58**, 2059 (1987).

[7] M. R. Krames, M. Ochiai-Holcomb, G. E. Holfer, C. Carter-Coman, E. I. Chen, I. H. Tan, P. Grillot, N. F. Gardner, H. C. Chui, J. W. Huang, S. A. Stockman, F. A. Kish, M. G. Craford, S. T. Tan, C. P. Kocot, M. Hueschen, J. Posselt, B. Loh, G. Sasser, and D. Collins, *Appl. Phys. Lett.* **75**, 2365 (1999).

[8] T. N. Oder, J. Shakya, J. Y. Lin, and H. X. Jiang, *Appl. Phys. Lett.* **83**, 1231 (2003).

[9] A. David, C. Meier, R. Sharma, F. S. Diana, S. P. DenBaars, E. Hu, S. Nakamura, and C. Weisbuch, *Appl. Phys. Lett.* **87**, 101107 (2005).

[10] S. Fan, P. R. Villeneuve, J. D. Joannopoulos, and E. F. Schubert,

Phys. Rev. Lett. **78**, 3294 (1997).

[11] M. Rattier, H. Benisty, R. P. Stanley, J.-F. Carlin, R. Houdré, U. Oesterle, C. J. M. Smith, C. Weisbuch, and T. F. Krauss, *IEEE J. Sel. Top. Quantum Electron.* **8**, 238 (2002).

[12] H. Rigneault, F. Lemarchand, and A. Sentenac, *J. Opt. Soc. Am. A* **17**, 1048 (2000).

[13] R. K. Lee, Y. Xu, and A. Yariv, *J. Opt. Soc. Am. B* **17**, 1438 (2000).

[14] P. R. Berman, New York:Academic, (1994)

[15] O. Painter, R. K. Lee, A. Scherer, A. Yariv, J. D. O`Brien, P. D. Dapkus, I. Kim, *Science*, **284**, 1819, (1999)

[16] H. G. Park, S. H. Kim, S. H. Kwon, Y. G. Ju, J. K. Yang, J. H. Baek, S. B. Kim, Y. H. Lee, *Science*, **305**, 1444, (2005)

[17] Y. S. Choi, K. Hennessy, R. Sharma, E. Haberer, Y. Gao, S. P. DenBaars, C. Meier, *Appl. Phys. Lett.*, **87**, 243101, (2005)

[18] E.M. Purcell *Phys. Rev.* 69, 681 (1946)

[19] C. M. Lai, H. M. Wu, P. C. Huang, S. L. Peng, *Appl. Phys. Lett.*, **90**, 141106, (2007)

[20] M. Imada, S. Node, A. Chutinan. and T. Tokuda, *Appl. Phys. Lett.*, **75**, 316, (1999)

[21] D. Ohnishi, T. Okano, M. Imada, and S. Node, *Opt. Exp.*, **12**, 1562, (2004)

Chapter 2

Fundamental theory of Photonic Crystal Surface Emitting Lasers

Introduction

A considerable amount of literature has been published on photonic crystal surface emitting lasers utilizing a 2D distributed feedback (DFB) mechanism [1-4]. The device features single longitudinal and transverse mode, lasing with large area and narrow beam divergence. To calculate photonic band-gap and the distribution of electric or magnetic field, there have been many theoretical analysis and methods developed, such as 2D plane wave expansion method (PWEM) [2,5], finite difference time domain (FDTD) [6,7], Transfer Matrix method and Multiple scattering method, etc. In this thesis, we focused on the lasing behavior of band-edge mode in GaN-based 2D PCSELs. Each of band-edge modes exhibits a different type of wave coupling according to the Bragg diffraction mechanism. In this chapter, we introduced the first and higher order Bragg diffraction in Chapter 2-1 and 2-2, respectively. According to Bragg diffraction mechanism, we expected emitted light angle would tilt an angle from normal direction.

2-1 First order Bragg diffraction in 2D triangular lattice PhCs[8,9]

Fig 2-1(a) shows a band diagram of a triangular-lattice photonic crystal. The

points (A), (B) and (C) are the points Γ_1, K_1, and M_1, respectively. The reciprocal space of the structure is a space combined by hexagons. Fig 2-1(b) shows a schematic diagram of a reciprocal space. The $\mathbf{K_1}$ and $\mathbf{K_2}$ are the Bragg vectors with the same magnitude, $|K|=2\pi/a$, where a is the lattice constant of the photonic crystal. Consider the TE modes in the 2-D photonic crystal structure, the diffracted light wave from the structure must satisfy the Bragg's law:

$$k_d = k_i + q_1 K_1 + q_2 K_2, \qquad q_{1,2} = 0, \pm 1, \pm 2, \ldots \tag{2.1}$$

$$\omega_d = \omega_i \tag{2.2}$$

where k_d is xy-plane wave vector of diffracted light wave, k_i is xy-plane wave vector of incident light wave, $q_{1,2}$ is order of coupling, ω_d is the frequency of diffracted light wave, and ω_i is the frequency of incident light wave. Equation (2.1) represents the phase-matching condition, and Equation (2.2) represents the constant-frequency condition (or energy conservation).

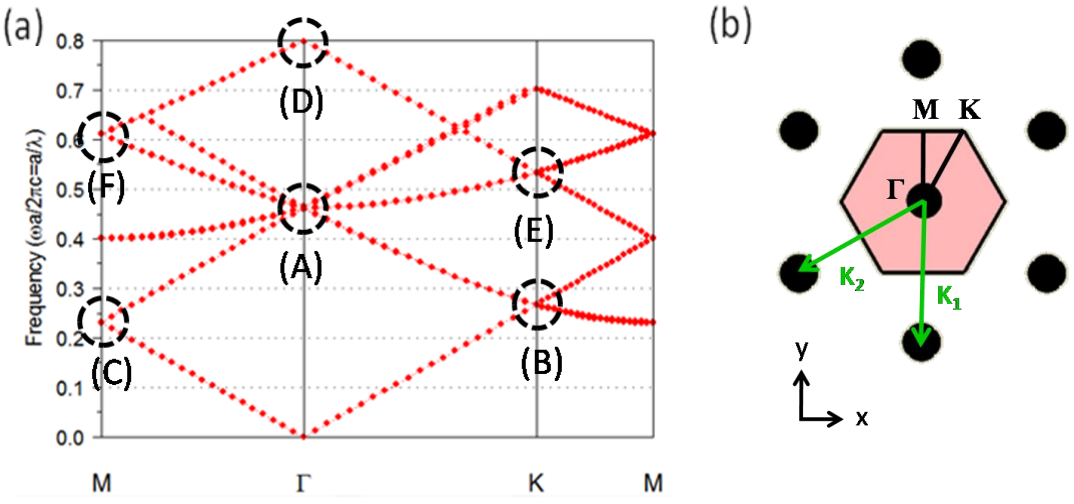

Figure 2-1(a)The band diagram of a triangular lattice photonic crystal; (b)The

schematic diagram of a reciprocal space.

It is expected lasing occurs at specific points on the Brillouin-zone boundary (Γ, M, and K) and at the points at which bands cross and split. At these lasing points, waves propagating in different directions couple to significantly increase the mode density. It is particularly interesting that each of these points exhibits a different type of wave coupling. For example, as shown in Fig 2-1(c), the coupling at point(C) only involves two waves, propagating in the forward and backward directions. This coupling is similar to that of a conventional DFB laser. However, there can be six equivalent Γ-M directions in the structure; that is, the cavity can exist independently in each of the three different directions to form three independent lasers. Point(B) has a unique coupling characteristic unachievable in conventional DFB lasers, the coupling of waves propagating in three different directions as shown in Fig 2-2(b). This means the cavity is a triangular. In fact, there can also be six Γ-K directions in the structure; therefore, two different lasing cavities in different Γ-K directions coexist independently. At point(A) the coupling includes waves in in-plane all six directions; 0°, 60°, 120°, -60°, -120°, and 180° as shown in Fig 2-2(a). In addition, the coupled light can be emitted perpendicular from the surface according to first order Bragg diffraction, as shown in Fig 2-3. This is the same phenomenon that occurs in conventional grating-coupled surface-emitting lasers. Therefore, the device functions

as a surface emitting lasers.

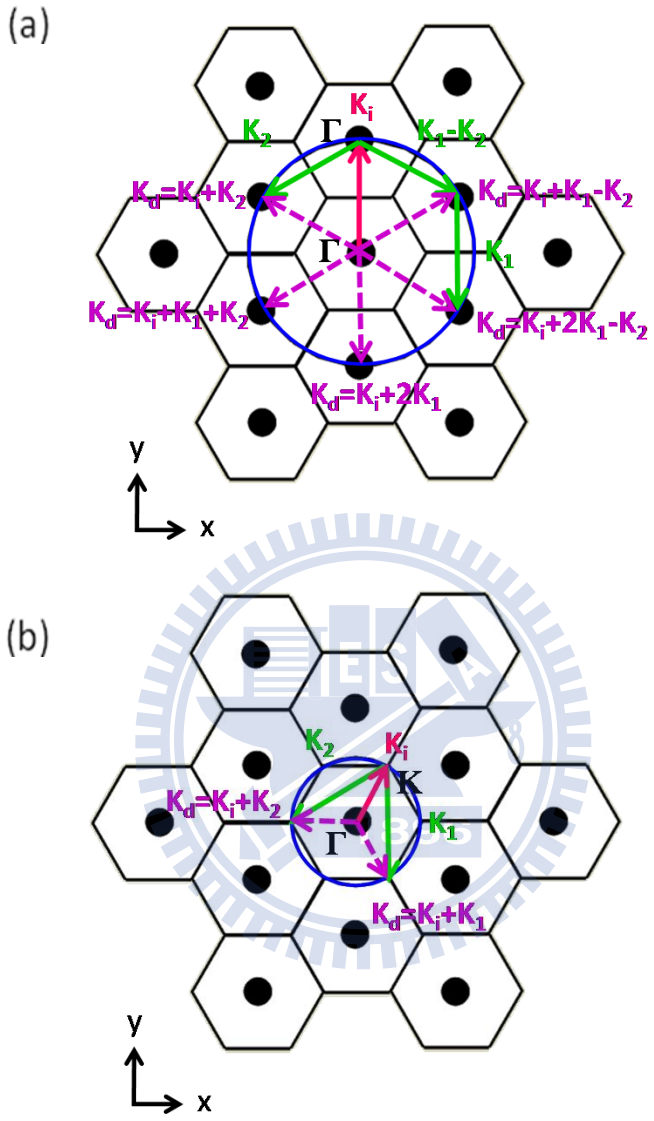

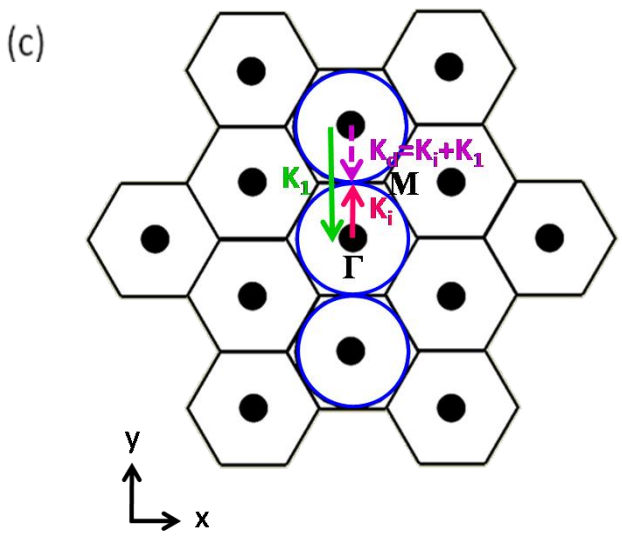

Figure 2-2 Wave vector diagram at points(A), (B), (C) in Figure 2-1(a), k_i and k_d indicate incident and diffracted light wave.

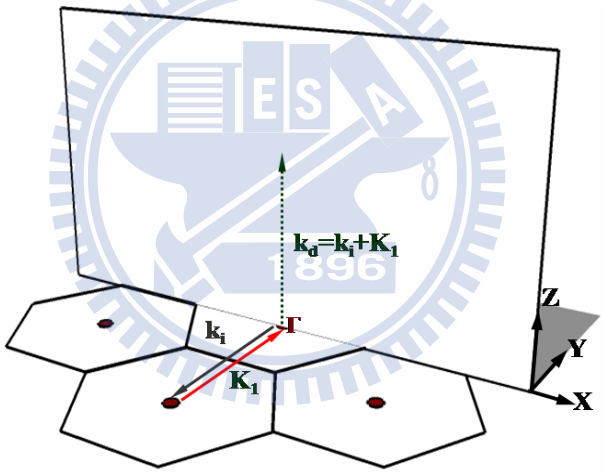

Figure 2-3 The wave vector diagram at point(A) in vertical direction.

2-2 Higher order Bragg diffraction in 2D triangular lattice PhCs

Fig 2-4(a) and Fig 2-4(b) show the in-plane and vertical diffraction at point(D). In this case, the light wave is diffracted in five Γ-K directions and in the vertical direction similar to point(A) and $(Ki+q_1K_1+q_2K_2)$ reaches the six Γ' points. Fig 2-4(c)

shows the wave-vector diagram of oneΓ’ point where the light wave is diffracted in an oblique direction. The light wave is also diffracted in a bottom oblique direction. The same diffraction phenomena occur at the other five G8 points, resulting in diffraction in 19 directions at point(D).

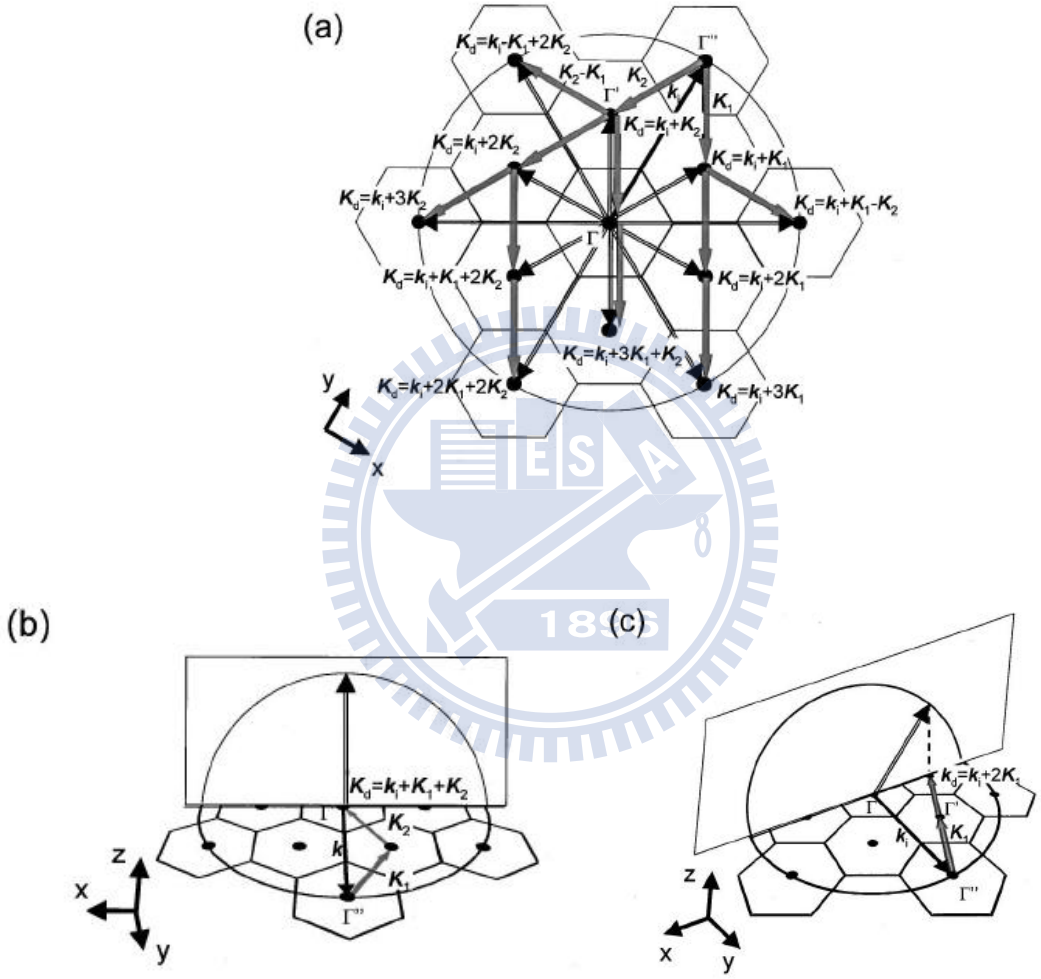

Figure 2-4 Wave vector diagram of (a)in-plane and (b)vertical direction at point(D); (c)wave vector diagram showing diffraction in an oblique direction at point(D).

Fig 2-5(a) and (b) show the in-plane and vertical diffraction at point(E). In this

case, the light wave is diffracted in three Γ-K directions and ($Ki+q_1K_1+q_2K_2$) reaches the three K' points. Fig 2-5(b) shows the wave-vector diagram of one K' point where the light wave is diffracted in an angle tilt 30° from normal direction. Therefore, we expect the lasing behavior of K2 mode would emit at this specific angle.

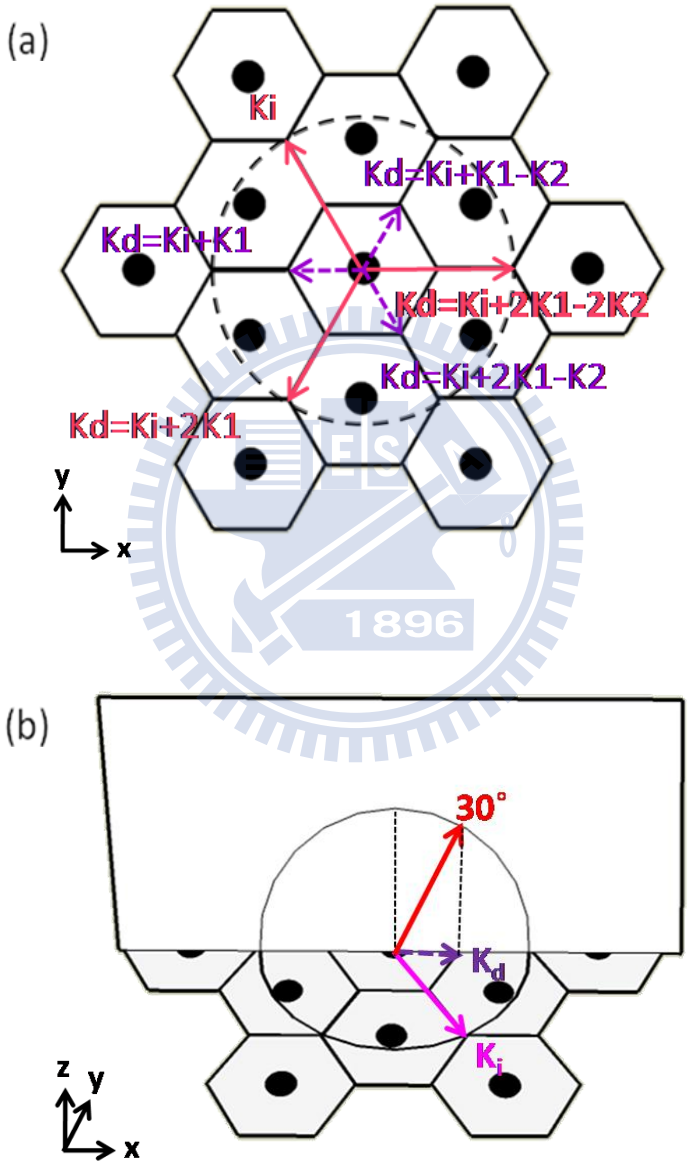

Figure 2-5 Wave vector diagram of (a)in-plane and (b)vertical direction at point(E) (or K2 mode), k_i and k_d indicate incident and diffracted light wave.

Fig 2-6(a) and (b) show the in-plane and vertical diffraction at point(F). In this case, the light wave is diffracted in two Γ-M directions and ($Ki+q_1K_1+q_2K_2$) reaches the three M' points. Fig 2-6(b) shows the wave-vector diagram of one M' point where the light wave is diffracted into three independent angles which tilts 19.47˚, 35.26˚, 61.87˚ from normal direction, respectively. Since we collected PL spectrum on one detected plane, these diffraction angles happened on different detected planes, we could only detect one diffraction angle at one time.

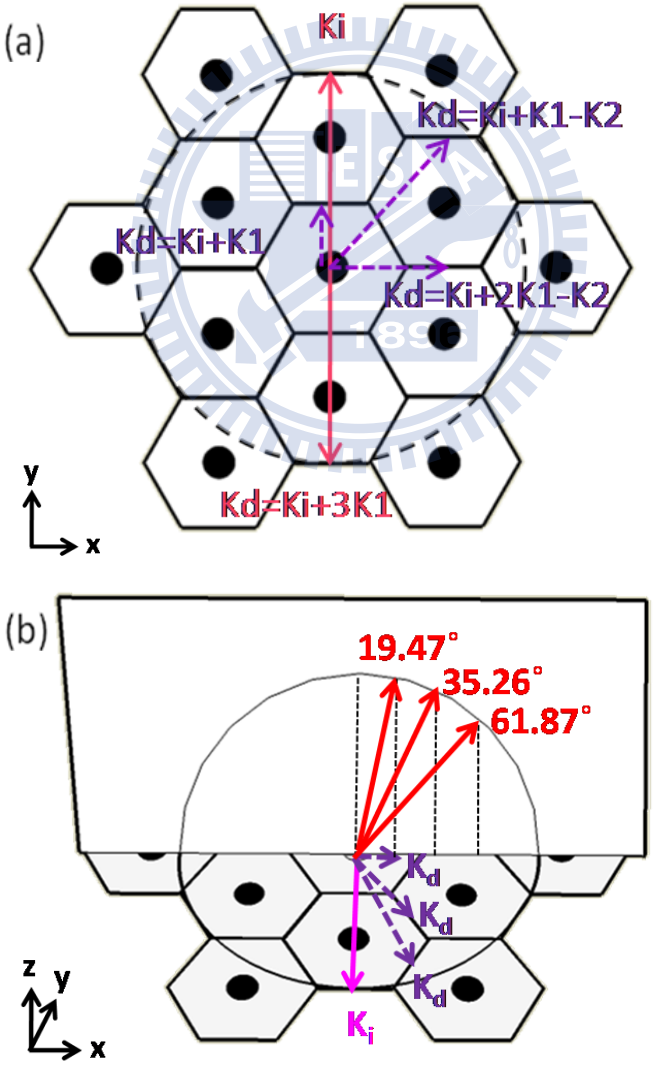

Figure 2-6 Wave vector diagram of (a)in-plane and (b)vertical direction at

point(F) (or M3 mode), k_i and k_d indicate incident and diffracted light wave.

2-3 Diffraction pattern of 2D PhCs [10]

In the previous section, we show the Bragg diffraction mechanism in independent mode. In this section, we talk about the continuous Bragg diffraction extraction in PhCs structure. Each direction of emission (or extraction) is associated with a given in-plane wave vector, *k//*, or effective index $n_{eff} = (k//)/k_0$, where k_0 is the wave vector of light in vacuum[11]. The components of the spectrum with effective index $n_{eff} < 1$ are extracted directly. These propagate in all directions in air and represent only 10% of the whole radiated power. The components with $1 < n_{eff} < 1.7$ are delocalized modes. These are produced by evanescent waves emitted by the dipole, and their contribution to the total radiated power is about 40%. The peaks in the dipole power spectrum with $1.7 < n_{eff} < 2.5$ are associated with guided modes, also induced by the dipole emission of evanescent waves. They carry slightly more than 45% of the total emission. The components with $n_{eff} > 2.5$ are purely evanescent and do not contribute in the radiated intensity.

The measurement covers all possible *k//* values in the light cone for each reduced frequency. For any given frequency, there is a discrete number of guided modes carried by the planar cavity, with $1.7 < n_{eff} < 2.5$. The lowest order mode has $n_{eff} < 2.5$.

This mode almost perfectly follows the GaN line, defined by $k// = 2.5k_0$. The number of guided modes as measured with this sample is in accordance with the simulation shown Figure 2-8(b). To explain all of the effects caused by a 2D PhC (in particular the effects related to polarization), the field, associated with a guided mode for example, should be described as a Bloch mode: $\mathbf{E}(\mathbf{r}) = \Sigma_{\mathbf{G}}\mathbf{E}_{\mathbf{G}} \bullet \exp[i(\boldsymbol{k}// + \mathbf{G}) \bullet \mathbf{r}]$, where $\mathbf{E}_{\mathbf{G}}$ is the electric field component corresponding to harmonic $\mathbf{G}$, and $\boldsymbol{k}//$ is the in-plane wave vector of the Bloch mode. With our PhC structure, the reciprocal lattice (RL) is a 2D triangular lattice rotated by 30° with respect to the direct lattice (DL) and RL vectors can be written as: $\mathbf{G} = h\mathbf{a}_1^* + k\mathbf{a}_2^*$, where h and k are integers, and $\mathbf{a}_1^*$ and $\mathbf{a}_2^*$ are the two RL basis vectors (Figure 2-7(b)). Harmonics of the Bloch mode are extracted if their in-plane wave vectors are within the light cone: $|\boldsymbol{k}// + \mathbf{G}| < k_0$. Bloch mode harmonics intensities decay like G^{-3} to infinity, with G the RL radial coordinate: high-order harmonics carry negligible intensity, and efficient extraction should involve low-order harmonics (associated with short RL vectors) in order to occur over reasonable lengths. The most striking feature observed in this plot is the detection of the radiative components of guided modes. The sets of lines labeled 2a and 2b in Figure2-7(a) are induced by the radiative harmonics of the TE-polarized guided modes propagating in the *ΓM* direction with in-plane wave vectors $\boldsymbol{k}// + \mathbf{G}_{10}$ and $\boldsymbol{k}// + \mathbf{G}_{-10}$ shown in Figure 2-7(b) , which only a radiative harmonic associated with set 2b.

The sets of lines labeled 3a and 3b are formed by the combination of two harmonics, as shown in Figure 2-7(b) (for a line associated with set 3a). These radiative harmonics are not associated with guided modes propagating in the *ΓM* direction but in directions about ±60°. The measurement of these components constitutes direct evidence of 2D PhC-assisted light extraction[12].

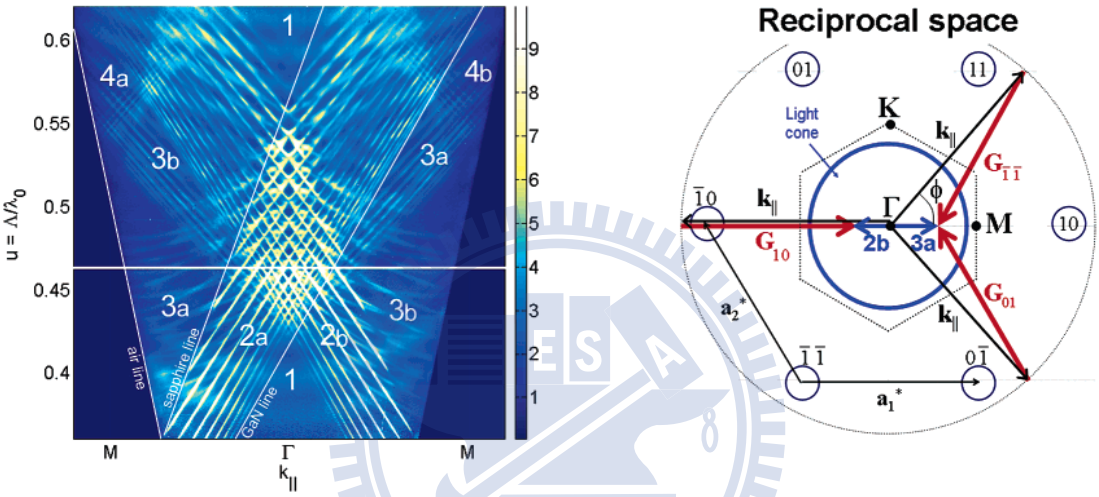

Figure 2-7(a)Normalized far-field PL spectrum of the PhC-assisted QD structure; (b)Reciprocal lattice associated with the 2D PhC and origin of extracted guided modes. The blue and gray circles indicate, respectively, the light cone and the trace of points with identical *k//*. The gray hexagon is the first Brillouin zone boundary.

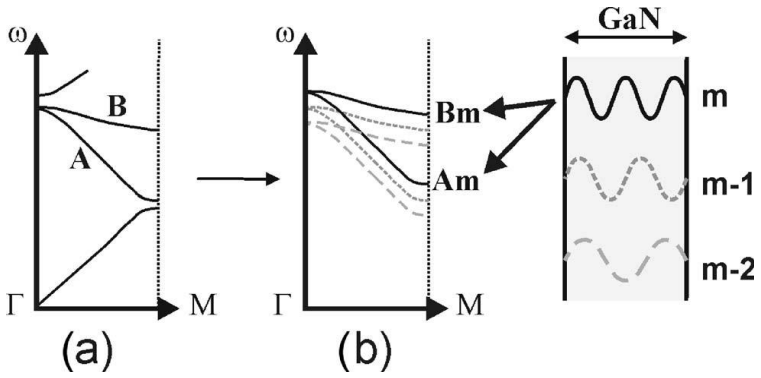

Figure 2-8(a)Two-dimensional band structure of a photonic crystal in the *ΓM* direction; (b)Corresponding band structure in a multimode waveguide: mode *m* gives rise to two PhC bands, *Am* and *Bm*.

2-4 Cavity mode and band-edge mode in 2D PhCs[13]

In this section, we introduce DFB laser model to explain the effect of defects in PCSELs. As shown in figure2-9, we apply 3 model of 2D DFB laser , by the couple mode theory and coupled in-plane wave equations , a set of evolution equations for the amplitude of the in-plane wave is obtained:

$$\begin{cases} \dfrac{dA}{dx} = uA - vBe^{2i\delta x} \\ \dfrac{dB}{dx} = -uA + vAe^{-2i\delta x} \end{cases}$$

where A and B are the amplitudes of the in-plane outward- and inward- propagating cylindrical waves, respectively x is the normalized radius x=βρ. δ=(βdesign–β)/β denotes the normalized frequency detuning factor. The coefficients u and v are defined as u=gA–h1,v=h1+ih2, where gA is the normalized gain coefficient. The

minimum value of gA required toachieve laser emission will be determined by the resonance condition. h1 and h2 are the radiation- and feedback- coupling coefficients, respectively

We consider reasonable boundary condition and calculate the ration of in-plane outward and inward propagation which indicated the reflection of the device. It shows the stop band and reflection spectrum in related to period of gatings as shown in figure 2-10(a). For different gain level, reflection will be greater than 100% gradually , we can clearly identify the band-edge mode and cavity mode when the gain coefficient gA>1×10-3 as shown in figure 2-10(b).

If we simplify defects in 2D PCSELs, it can be treated as 1D DFB laser with localized defect , in other words , 1D DFB laser cavity detuning with different cavity length. Then the lasing wavelength and threshold between different defects in PCSELs match the simulation results.

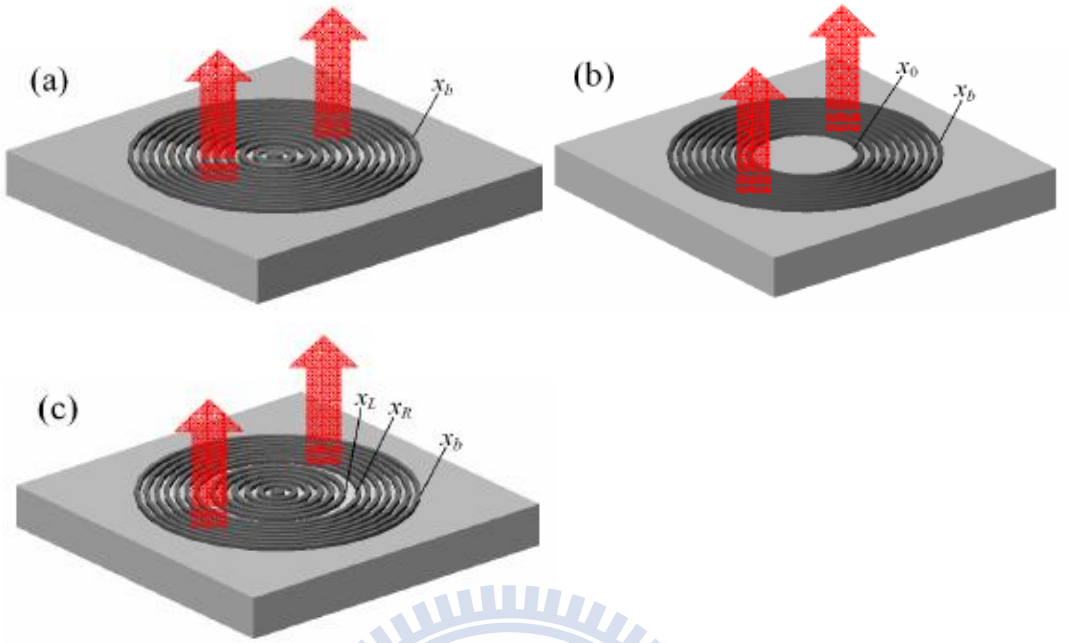

Figure 2-9(a)Circular DFB lasers;(b)Dick Bragg resonator laser;(c)Ring Bragg resonator laser. Laser radiation in coupled out of the resonator in vertical direction via the graings

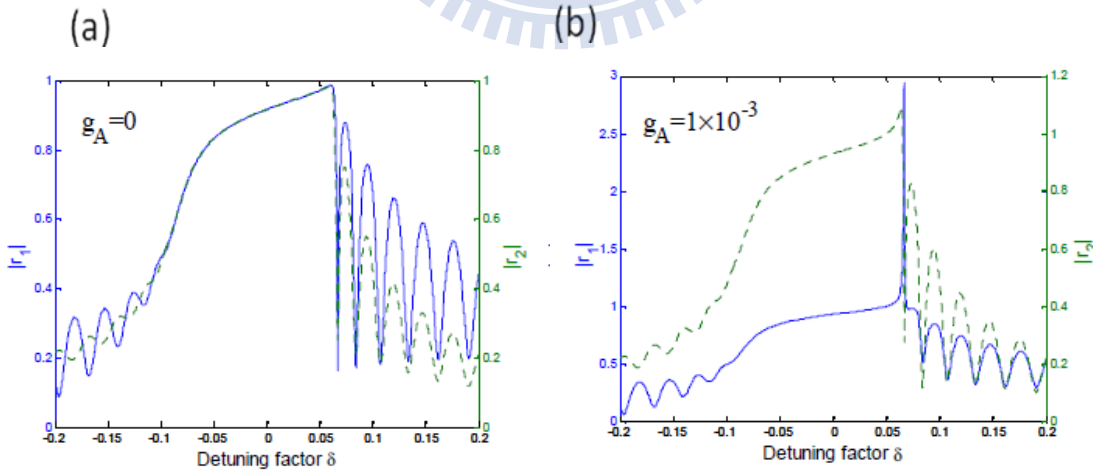

Figure 2-10 Reflection for different gain level (a) gA=0, (b) 1×10-3, in the presence of vertical radiation.

References

[1] M. Imada, S. Noda, A. Chutinan, T. Tokuda, M. Murata, and G. Sasaki, *Appl. Phys .Lett*. **75**, 316 (1999)

[2] S. Noda, M. Yokoyama, M. Imada, A. Chutinan, and M. Mochizuki, *Science* **293**, 1123 (2001)

[3] H. Y. Ryu, S. H. Kwon, Y. J. Lee, and J. S. Kim, *Appl. Phys. Lett.* **80**, 3467 (2002)

[4] G. A. Turnbull, P. Andrew, W. L. Barns, and I. D. W. Samuel, *Appl. Phys. Lett.* **82**, 313 (2003)

[5] K. Sakai, E. Miyai, T. Sakaguchi, D. Ohnishi, T. Okano, and S. Noda, *IEEE J. Sel. Areas Commun.* 23, 1335-1340 (2005)

[6] M. Imada, A. Chutinan, S. Noda and M. Mochizuki *Phys. Rev. B* **65**, 195306 1-8 (2002)

[7] M. Yokoyama and S. Noda *Opt. Express* **13**, 2869-2880 (2005)

[8] M. Imada, A. Chutinan, S. Noda, M. Mochizuki, *Phy. Rev. B*, 65, 195306 (2002)

[9] M. Notomi, H. Suzuki, and T. Tamamura, *Appl. Phys. Lett.*, **78**, 1325 (2001)

[10] Fre´de´ric S. Diana, Aure´lien David, Ines Meinel, Rajat Sharma, Claude Weisbuch, Shuji Nakamura and Pierre M. Petroff, *Nano Lett.*, Vol. **6**, 1116-1120 (2006)

[11] Soller, B. J.; Stuart, H. R.; Hall, D. G. *Opt. Lett.*, **26**, 18, 1421 (2001)

[12] A. David, C. Meier, R. Sharma, F. S. Diana, S. P. DenBaars, E. Hu, S. Nakamura, C. Weisbuch, H. Benisty, *Appl. Phys. Lett.*, ***87***, 101107 (2005)

[13] Xiankai Sun and Amnon Yariv , *Optics Express* , **16** ,9155 (2008)

Chapter 3

Fabrication of Nitride-based 2D Photonic Crystal Surface Emitting Lasers

3-1 Electron-Beam Lithography System(EBL)

Recently, photonic crystals, which are periodic patterns with sizes of nano-scale, are usually fabricated using electron-beam lithography. The first EBL machine, based on the scanning electron microscope(SEM) mechanism, was developed in the 1960s. The technique of EBL is using electron beam to generate patterns on a surface and the De-Broglie relationship(λ <0.1nm for 10-50keV electrons) to avoid the diffraction limit. Therefore, we can overcome the diffraction limit of light and create nano-scale pattern without mask by using this technique. The EBL system usually consists of an electron gun for generating electron beam, a beam blanker for controlling the electron beam, electron lenses for focusing the electron beam, a stage and a computer control system as shown in Figure 3-1.

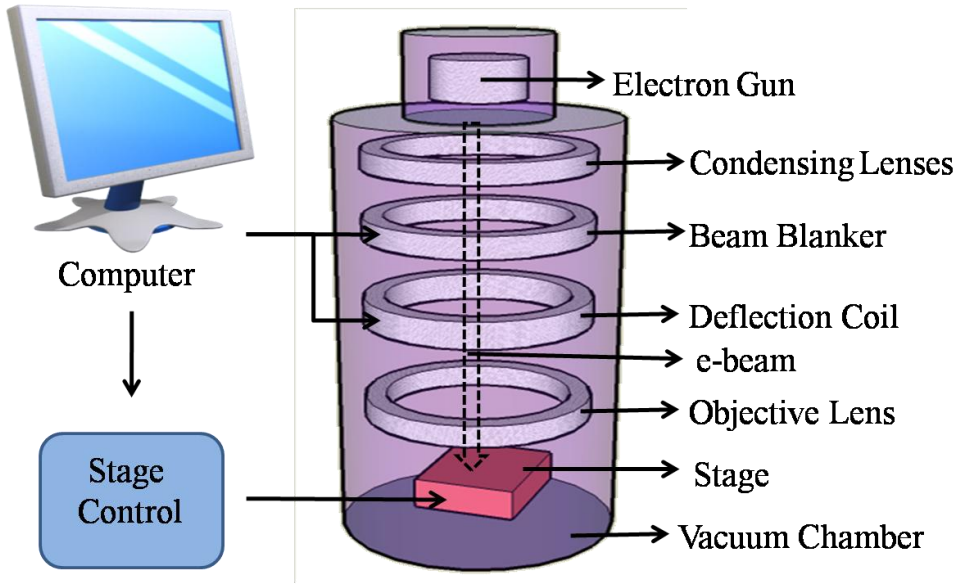

Figure 3.1 The typical schematic diagram of EBL system.

Electron sources

Electrons can be emitted from a conductor either by heating the conductor with a sharp point where the electrons obtain sufficient energy from the thermal source to overcome the work function of the conductor(thermal emission sources) or by applying a strong electric field where the electrons can tunnel through the work function(field emission sources). There are three key parameters of the electron source such as actual spot size on sample, brightness and the electrons possess wide range of energy. Where the actual spot size is determined by the number of the lenses; brightness is similar to the intensity of light, that is the brighter the electron source has a higher current in the electron beam.

Table 3-1 shows different types of electron sources. For our system, we use

"Thermal (Schottky) Field Emitter" as electron source. It combines a field emission source with sharp tungsten and the heating of the thermal source. Due to the source tip operates at 1800K, it is less sensitive to environmental gases and can achieve stable operation for months.

Sources	Spot size (μm)	Brightness (A/cm2/sr)	Vacuum requirement (Torr)
Tungsten Thermionic	25	~10^5	10^{-6}
Thermal(Schottky) Field Emitter	20	~10^8	10^{-9}
Cold Field Emitter	5	~10^9	10^{-10}

Table 3-1 The properties of electron sources

Electron lenses

Since the electronic or magnetic field can control the electron beam path, we called them "electron lenses". Although we can imagine electron lenses as optical lenses, the electron lenses have shortage in ability of aberrations calibration, especially spherical aberration and chromatic aberration. To minimize the influence caused by aberration, the electron beam should always confine at the center of lenses.

Beam blanker

The function of beam blanker is turn on or off the electron beam. It usually consists of a pairs of plates as a electronic deflector. Either or both plates are linked to a blanking amplifier with a fast response time. The voltage is applied across the plates to turn the beam off. This function is necessary for moving the beam from one designed structure to another with no leaky electron beam current.

Stage and computer control system

The stage provides high resolution movement of sample and we use the computer control system to dominate the movement of stage. Besides, the computer control system can design the e-beam lithography pattern by GDS software.

3-2 Wafer Preparation

The nitride heterostructure of GaN-based MCLED was grown by metal-organic chemical vapor deposition (MOCVD) system (EMCORE D-75) on the polished optical-grade c-face (0001) 2'' diameter sapphire substrate, as shown in Figure 3-2. Trimethylindium (TMIn), Trimethylgallium (TMGa), Trimethylaluminum (TMAl), and ammonia (NH_3) were used as the In, Ga, Al, and N sources, respectively. Initially, a thermal cleaning process was carried out at 1080°C for 10 minutes in a stream of hydrogen ambient before the growth of epitaxial layers. The 30nm thick GaN nucleation layer was first grown on the sapphire substrate at 530^{o}C, then 2μm thick

undoped GaN buffer layer was grown on it at 1040°C. After that, a 35 pairs of quarter-wave GaN/AlN structure was grown at 1040°C under the fixed chamber pressure of 100Torr and used as the high reflectivity bottom DBR. Finally, the 5λ active pn-junction region was grown atop the GaN/AlN DBR, composed typically of ten $In_{0.2}Ga_{0.8}N$ quantum wells (L_W=2.5 nm) with GaN barriers (L_B=7.5 nm), and surrounded by 560nm thick Si-doped n-type GaN and 200nm thick Mg-doped p-type GaN layers.

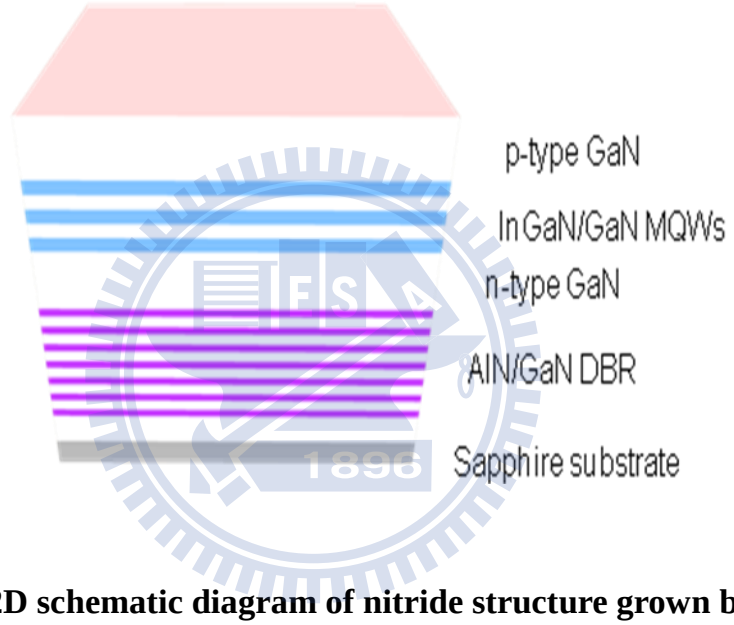

Figure 3-2 The 2D schematic diagram of nitride structure grown by MOCVD.

3-3 Process Procedure

There are some principles to fabricate GaN-based PCSELs, including initial clean (I.C.), plasma enhanced chemical vapour deposition (PECVD) technique, EBL technique and inductively coupled plasma - reactive ion etching (ICP-RIE) technique. The purpose of the I.C. is to remove the small particle and organism on the sample surface. The steps of I.C. are described as below.

Initial clean (I.C.)

1. Degreasing particles in acetone (ACE) 5min by ultrasonic baths.
2. Dipping in isopropyl alcohol (IPA) 5min by ultrasonic baths for organism removed.
3. Rising in de-ionized water (D.I. water) 5min for surface clean.
4. Blowing with N_2 gas for surface drying.
5. Baking by hot plate 120^{o}C, 5min, for wafer drying.

PECVD (SAMCO PD220)

The purpose of PECVD technique is to deposit a SiN film for hard mask. The details of PECVD parameters are expressed as below.

1. Initial clean
2. SiN film deposition :

   $SiHl_4$/Ar : 20sccm

   NH_3 : 10sccm

   N_2 : 490sccm

   Temperature : 300℃

   RF power : 35W

   Pressure :100Pa

   Time : 20min for depositing SiN 200nm

EBL

The purpose of the EBL is to define the PC pattern on the photoresist (PMMA) (soft mask). In the process of EBL, a special positive photoresist PMMA (A3) was used. These EBL parameters are described as below.

1. Spin coating use the photoresist : PMMA (A3).

a. first step : 1000 rpm for 10sec.

b. second step : 5000 rpm for 90sec.

2. Hard bake : hot plate 180^{o}C, 1hr.

3. Exposure :

   Beam voltage : 10KeV

   Writefield size : 50μm

4. Development : dipping in IPA : MIBK(3 : 1) 50sec.

5. Fixing : rising in IPA 30sec.

6. Blowing with N_2 gas for drying.

7. Hard bake : hot plate 120^{o}C, 4min.

8.

ICP-RIE (Oxford Plasmalab system 100)

The soft mask was transfered to SiN film to form the hard mask by using ICP-RIE. These ICP-RIE techniques are described as below.

1. SiN film etching:

   Ar/O_2: 5sccm

   CHF_3: 50sccm

   Forward power: 150W

   Pressure: 7.5*10^{-9}Torr

   Temperature: 20℃

   Time: 100 second for etching SiN film 200nm

2. Initial clean for remove soft mask

ICP-RIE (SAMCO RIE-101PH)

The purpose of the ICP-RIE techique is to form the PC layer on GaN. The hard

mask was transferred to GaN by using ICP-RIE techique. Figure 3-4 are shown the SEM image of top view and cross section of completed 2D PCSELs, respectively. These ICP-RIE techniques are described as below.

1. P-GaN etching:

   Ar : 10sccm

   Cl_2 : 25sccm

   ICP power : 200W

   Bias power : 200W

   Pressure : 0.33Pa

2. Dipping BOE 40sec. for remove hard mask

3. Polishing sapphire for optical pumping

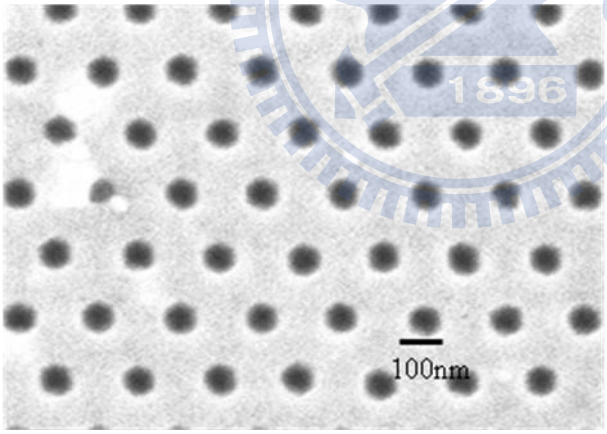

Figure 3-3 SEM images of plane view.

3-4 Process flowchart

The PCSELs was fabricated by following process steps. In the beginning, the hard mask SiN 200nm was deposited by PECVD. Then PMMA layer (150nm) was

spun by spinner and exposed using E-beam writer to form soft mask. The pattern on soft mask was transferred to SiN film to form the hard mask by using ICP-RIE (Oxford Plasmalab system 100), and then the PMMA layer was removed by dipping ACE . The pattern on hard mask was transferred to GaN by using ICP-RIE (SAMCO RIE-101PH) to form the PC layer. Finally, the sample dips in BOE to remove the hard mask.

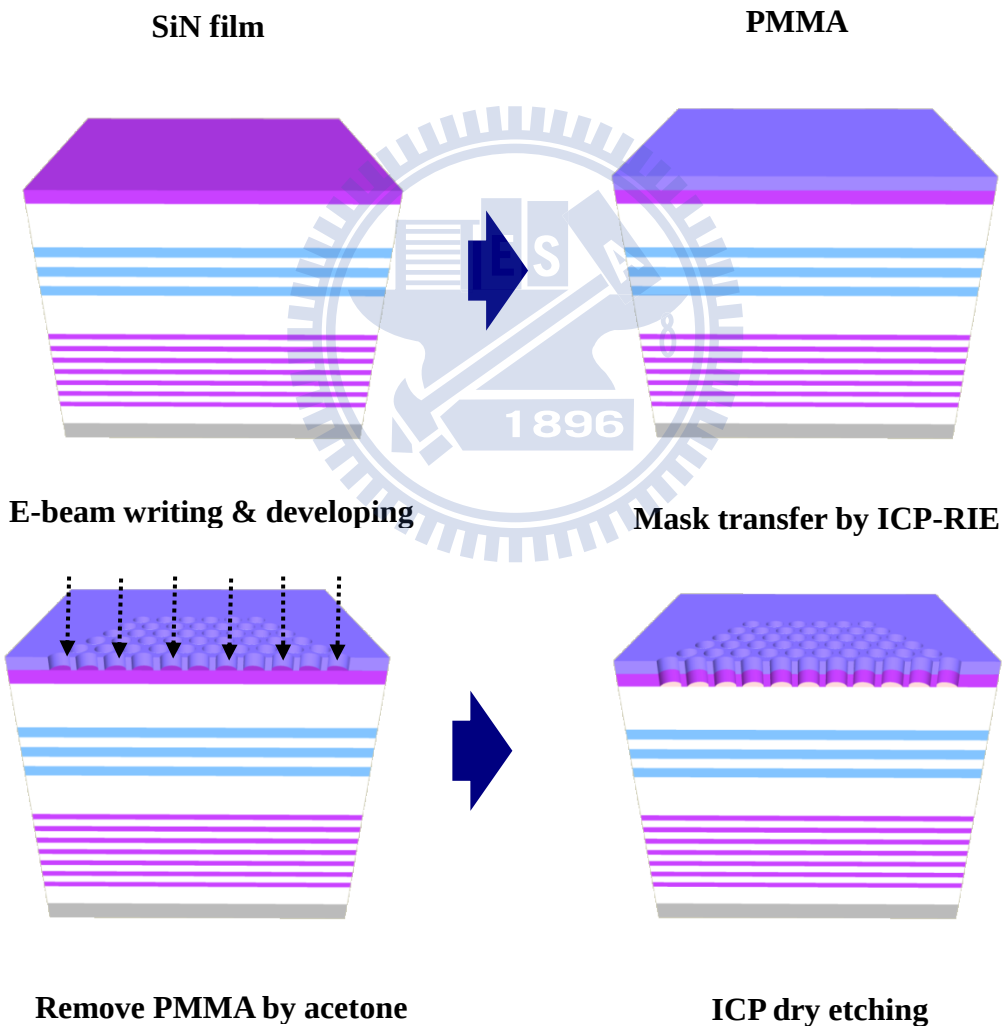

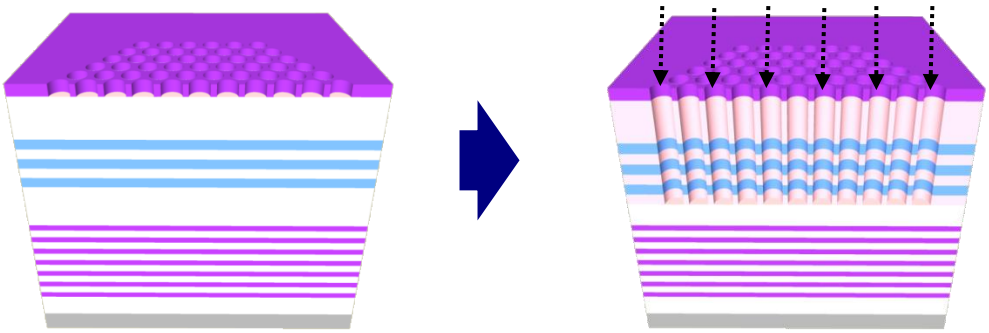

Figure 3-4 Process flowchart of PCSELs.

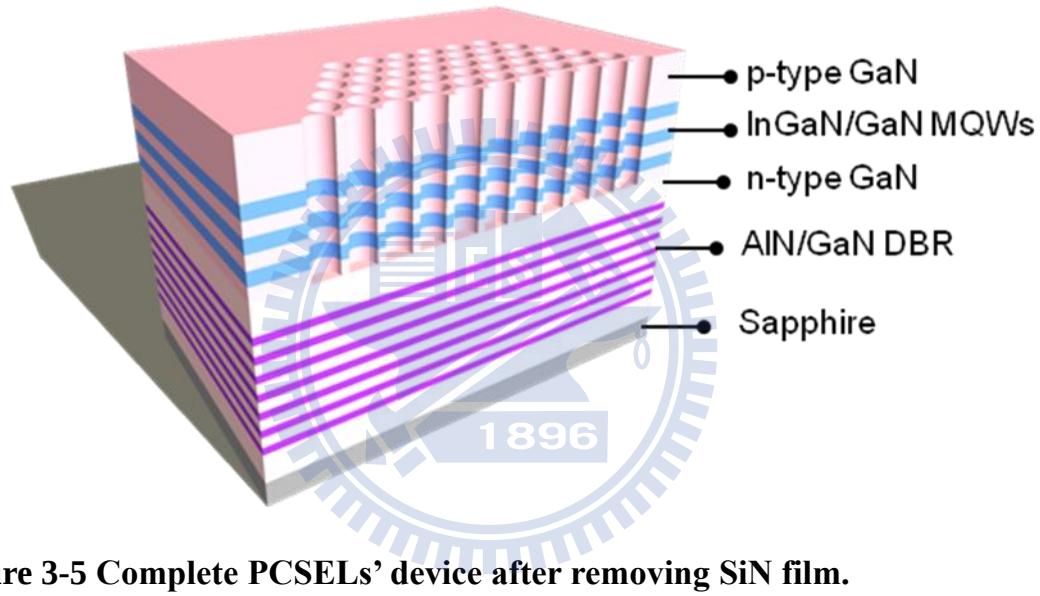

Figure 3-5 Complete PCSELs' device after removing SiN film.

To completely describe the process flowchart, each process conditions are entirely listed in the Table 3-2.

Step	Process	Conditions
1	Soft mask	(1) I.C. (2) Deposit 200nm SiN by PECVD.

		(3) Spin 150nm PMMA by spinner **(4) Define PCSELs pattern by EBL.** **(5) Development.** **(6) Hard bake**
2	**Hard mask**	**(1) Dry etching by ICP-RIE (Oxford Plasmalab system 100) to form the hard mask.** **(2) Remove PMMA by ACE.** **(3) Hard bake.**
3	**PCSELs**	**(1) Dry etching by ICP-RIE ((SAMCO RIE-101PH) to transfer the hard mask to GaN.** **(2) Remove hard mask by BOE.** **(3) Hard bake.**

Table 3-2 Detailed process flowchart of PCSELs

3-5 The design for PCSELs

In this section, we focus on the design for our GaN-based 2D PCSELs. Initially, we calculate the TE like mode dispersion band diagram to determine the normalized frequency which we choose for specific band-edge groups. Normalized frequency is the ratio of the wavelengths of optical modes and the lattice constants in PC. Once the

lasing wavelength is determined, the lattice constant is certain to be determined. The lasing wavelength is located within the emission of the active layer. According to the theory described in chapter 2, the surface emitting laser in the photonic crystal grating structure could only happen as the Bragg condition is satisfied. In additional, the Bragg condition is satisfied at Brillouin zone boundary, Γ, K and M point. At these points, light waves have opportunity to diffract normally to the surface which was described in section 2.2. Therefore, we can design a GaN-based 2D PCSEL operating at the designed lasing wavelength with the optimized lattice constant at Brillouin zone boundary, Γ, K and M point, which can be defined in the photonic band diagram.

In this study, we fix the parameter, r/a, to be 0.21 for calculating the band diagram of PC using 2D plan wave expansion method (PWEM). In fact, the 2D PWEM couldn't precisely evaluate the photonic band diagram of our 3D structure. That means we should do some modification to parameters describing our structure and then bring them into the 2D PWEM to approximate real condition. Therefore, according to reference [1], we further bring two parameters which are confinement factor (Γ_g) and effective refractive index (n_{eff}) into our calculation. Γ_g is the ratio of the light confined within the 2D PC structure to the light inside the whole device, and n_{eff} is the effective refractive index of the entire device with PC that take into account the effects of partial modal overlap of electromagnetic fields. Γ_g and n_{eff} could be used to estimate

the effective dielectric constant of nano-hole (ε_a) and the background (ε_b) for 2D PWEM calculation to further approximate the 3-D structure. These two parameters can be obtained by solving the distribution of the electric field in the in-plane direction. The Γ_g and n_{eff} for describing our structure are estimated to be 0.8284 and 2.5 considering fundamental mode, respectively. It is first estimated by transfer matrix method and shown in Figure 3-6.

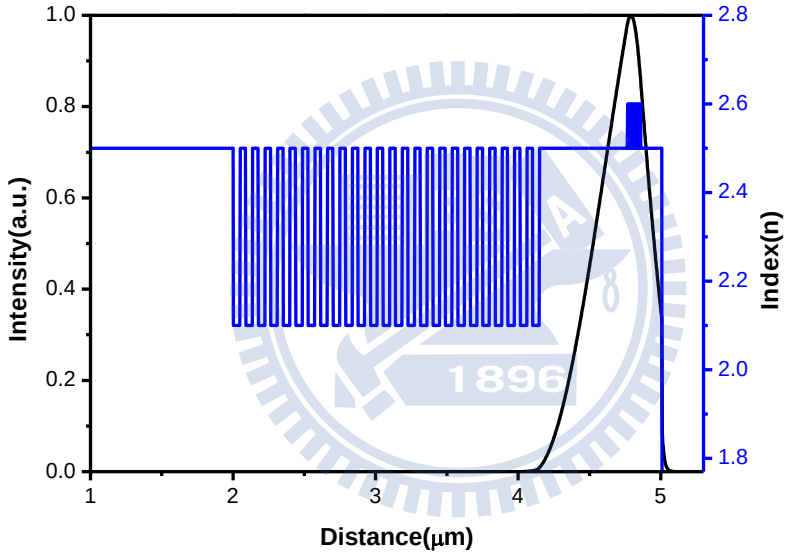

Figure 3-6 The lowest guided mode optical field distribution, where the confinement factor Γ=0.8284 and n_{eff}=2.5.

Then, we could determine ε_a and ε_b using two conditions:

$$n_{eff}^{\ 2} = f\varepsilon_a + (1-f)\varepsilon_b \tag{3.1}$$

$$\Delta\varepsilon = \varepsilon_b - \varepsilon_a = \Gamma_g(\varepsilon_{mat} - \varepsilon_{air}) \tag{3.2}$$

where the *f* is a filling factor, ε_{mat} is the dielectric constant of semiconductor, and ε_{air} is the dielectric constant of air. For a triangular lattice PC, *f* is written as:

$$f = \frac{2\pi r^2}{\sqrt{3}a^2} \tag{3.3}$$

Therefore, the value of ε_a and ε_b in unit cell for our PC device could be obtained to be 4.11 and 7.07, respectively. To bring ε_a and ε_b into the calculation, a band diagram of the 2D triangular lattice PC structure for TE like mode with r/a=0.21 on our sample structure could be estimated as shown in Fig 3-7. The figure shows that the each mode dispersion curve cross and splits at specific band-edges, the mode density is higher at those boundaries, light at these areas can propagate along different direction and have chance to couple and form a laser cavity. According to the theory described in chapter 2, the surface emitting behavior in the photonic crystal grating structure could only happen as the Bragg condition is satisfied.

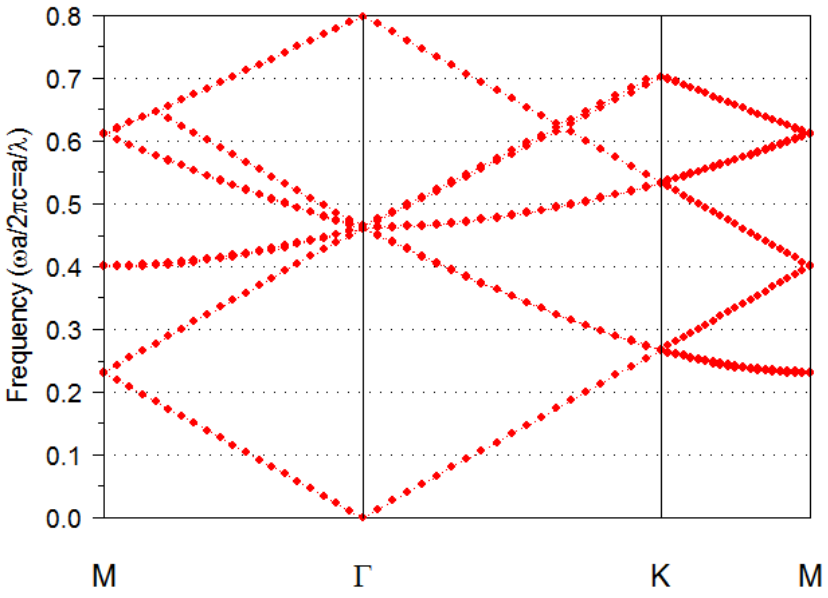

Figure 3-7 The TE band dispersion diagram of our design.

In order to have a high opportunity to meet those modes satisfying Bragg condition, the lattice constant of photonic crystal were determined to 190nm considering a PL peak wavelength of 400 nm which pumped by YVO4 laser (laser wavelength=355nm) and HeCd laser (laser wavelength=325nm) .

Chapter 4

Optical Characteristics of GaN-based 2D Photonic Crystal Surface Emitting Lasers with Localized Defects

4-1 Optical pumping system (Angle-resolved μ-PL)

The angle-resolved μ-PL (AR μ-PL) system is designed for multiple uses. As shown in Figure 4-1, we have two optical pump sources, two optical pump incidence paths, two collecting PL method and two way to collect sample surface image. The two optical pump sources are: one is frequency tripled Nd:YVO_4 355nm pulsed laser with a pulse width of ~0.5ns at a repetition rate of 1KHz; the other is 325 nm HeCd continuous wavelength laser. The samples are optically pumped by laser beam with an incident angle of 0° or 60° to the sample. The laser spot size is about 50μm in diameter so that covering the whole PhCs pattern area. The PL is collected by a 15X objective lens and straightly collected by spectrometer with a charge-coupled device (Jobin-Yvon IHR320 Spectrometer) or collected by a fiber with a 600μm core, which rotating in the normal plane of the sample, and also coupled into spectrometer. The spectral resolution is about 0.07nm for spectral output measurement. Figure 4-1 shows the setup of our AR μ-PL system. The GaN-based PCSELs were placed in a

cryogenics controlled chamber for performing PL experiment under low temperature (in order to prevent damage caused by heat). We can also monitor the image and spatial distribution on the sample surface by charge-coupled device (CCD) and beam view, respectively.

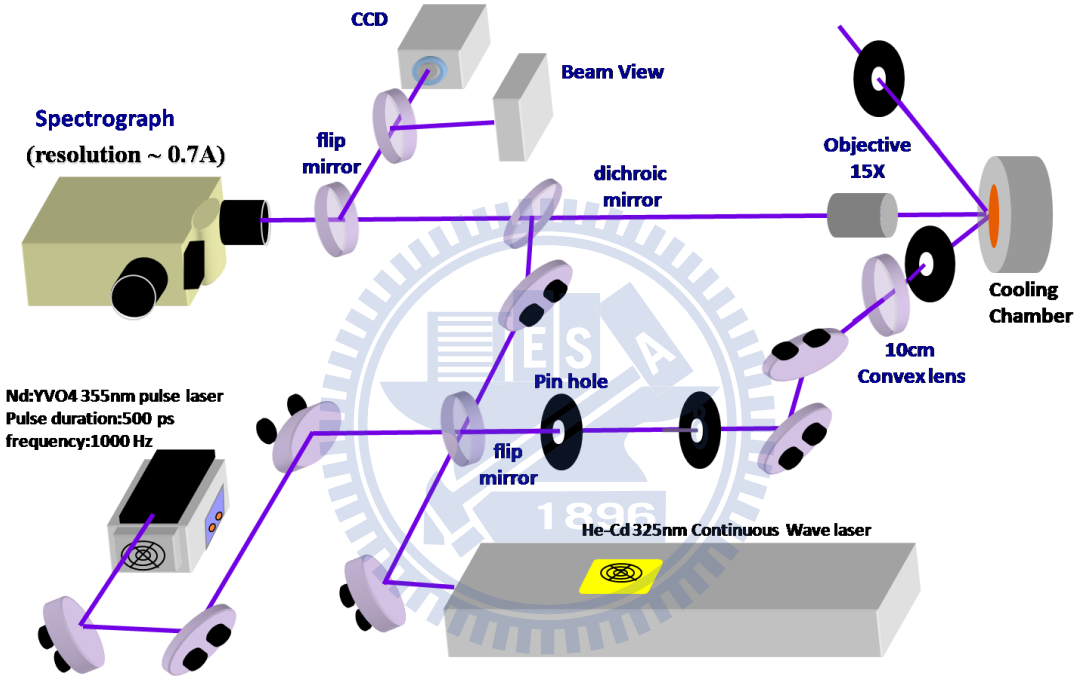

Figure 4-1 The angle-resolved μ-PL (AR μ-PL) system.

4-2 Data normalization

We set up a rotational stage just under the sample stage to measure the light field distribution which emitted by PCSELs. In this way, the rotation center would match the sample center roughly. We have a detected arm connected the rotational stage and the fiber detector. Rotating the rotational stage, the fiber could collect PL spectrum at

different angle. Therefore, we have a series of PL spectra distributed in continuous space, we named these spectra as “angle-resolved μ-PL” (AR μ-PL).

After measurements, we transformed the AR μ-PL spectra to obtain the guided modes dispersion relationships (reduced frequency $u=\Lambda/\lambda_0$ as y-axis versus in-plane wave vector, $k//$, as x-axis), by using the relation $k// = k_0 \sin\theta$. In addition, for each wavelength, $I_{PL}(\tilde{o})$ is normalized relative to its integrated intensity[1]. The resulting normalized AR μ-PL diagram, shown in Figure 4-2, reveals the dispersion relationships of guided modes and points to details about their relative excitation and out-coupling efficiency.

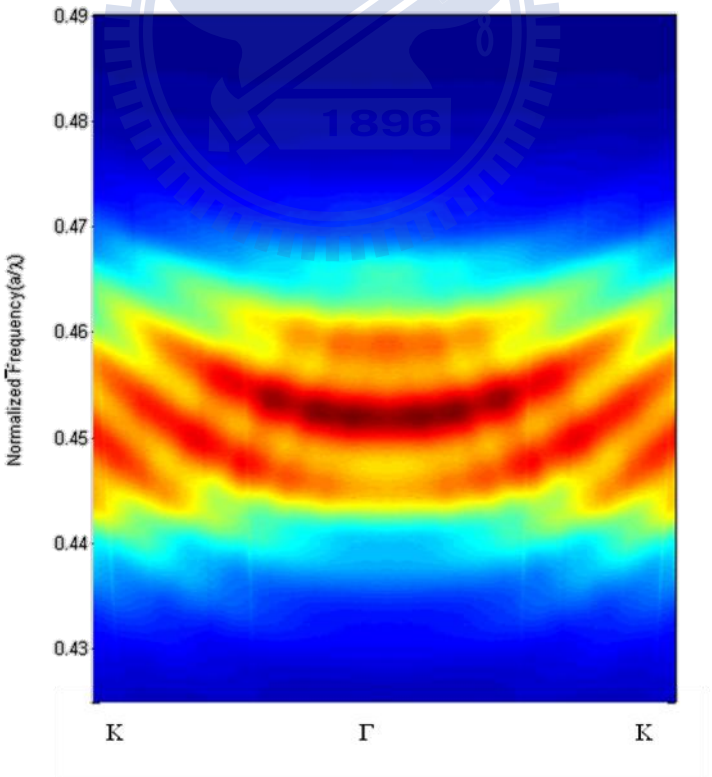

Figure 4-2 The AR μ-PL diagrams where the colorbar represents intensity and relative intensity with log value, respectively.

4-3 Experimental results of different defects of PCSELS

Our group has successfully demonstrated the PCSELs with different defects structure. Figure 4-3 are the SEM images of different defects. From the SEM image, defects in PCSELs are classified into four type , one is without defect, the other is with 3 period missing (H3) Fig4-3(b), the other is with 4 period missing (H4) Fig4-3(c), another is with 5 period missing (H5) Fig4-3(d).

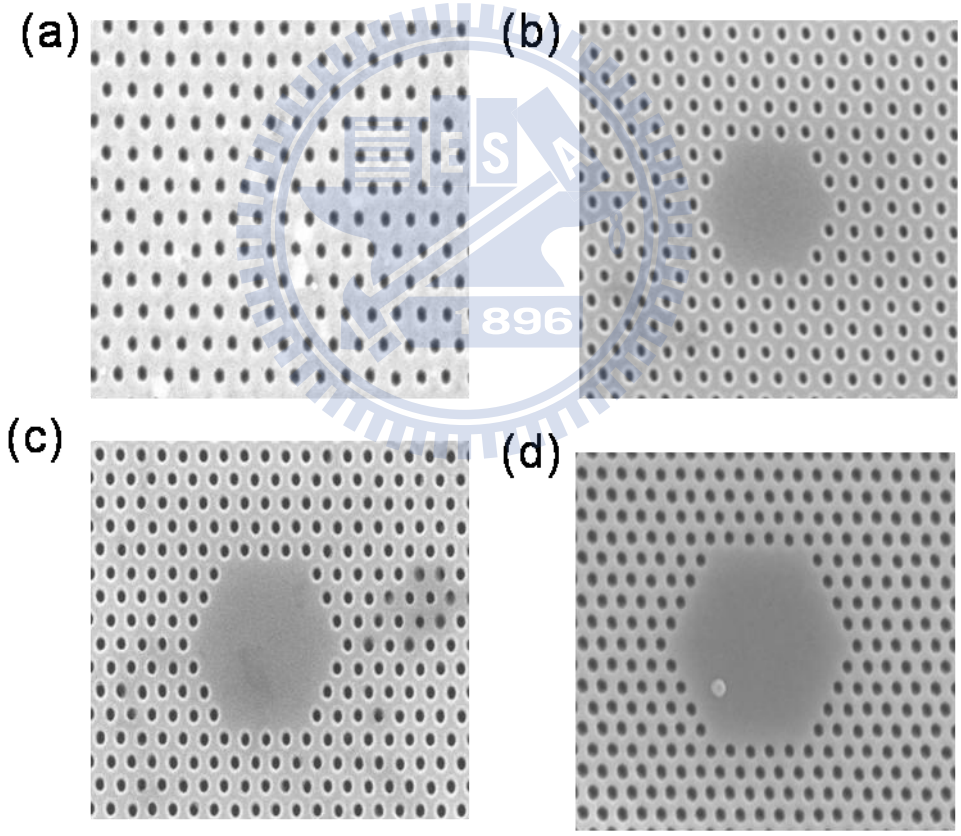

Figure 4-3 SEM of (a)H0 (b)H3 (c)H4 (d)H5 PCSELs.

In order to differentiate the influence caused by defects from the diffraction pattern caused by PhCs, we measured AR μ-PL diagrams for four structures

mentioned above. We simulated the fundamental guided mode by waveguide theory in our structures as in Figure 4-4(a). Further, we also simulated light field distributions for higher order guided modes. Figure 4-4 (b)show the confinement factor, which is the light field confined in the PhCs region over the light field in the entire structure, versus guided modes in different pairs of DBR. It's clear that the confinement factor has increased obviously at 25 pairs of DBR. Therefore, the standard structure of PCSELs is fabricated with 25 pairs of DBR pairs.

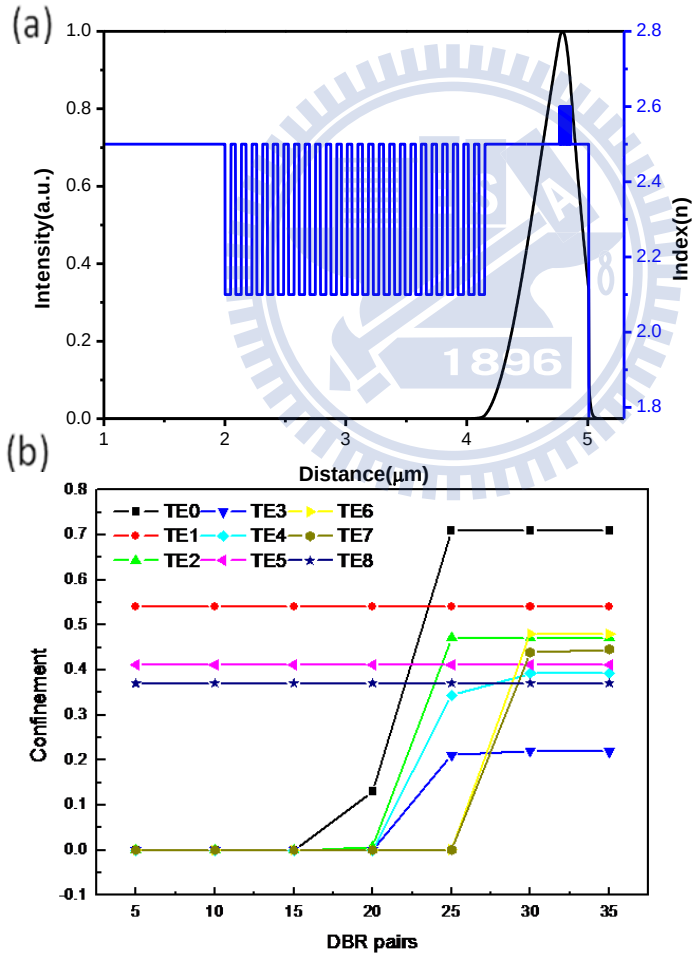

Figure 4-4 The confinement factor of guided modes in different pairs numbers of DBR structure.

Figure 4-5 is the AR μ-PL diagrams of different defects of PCSELs. Two kinds of modes are observed: Fabry–Pérot modes (background broad curves), present in any planar structure with embedded MQWs and DBR structure, and guided modes diffracted by the PhCs (sharp lines) corresponding to an enhancement on the total emitted light due to the PhCs on the surface. Since those emitted light are guided modes coupled with band structure, these lines clearly clarify the characteristics of PhCs. We simulated the band structure by RSoft commercial software using the parameters of the exact PCSEL device we measured and mapped the band structure with the AR μ-PL diagram. Since the slope of diffraction lines in both AR μ-PL diagrams show good agreement with the same band structure, we can tell that the PhCs structures show the same slope of diffraction lines if they own the same characteristics(ex. r/a ratio).Then we fit the guided modes dominated in our PCSELs , and it exhibited the band structure for different defects of PCSELs (Figure4-6).From the mapping band diagram , we find that their diffraction characteristics are similar for different PCSELs.

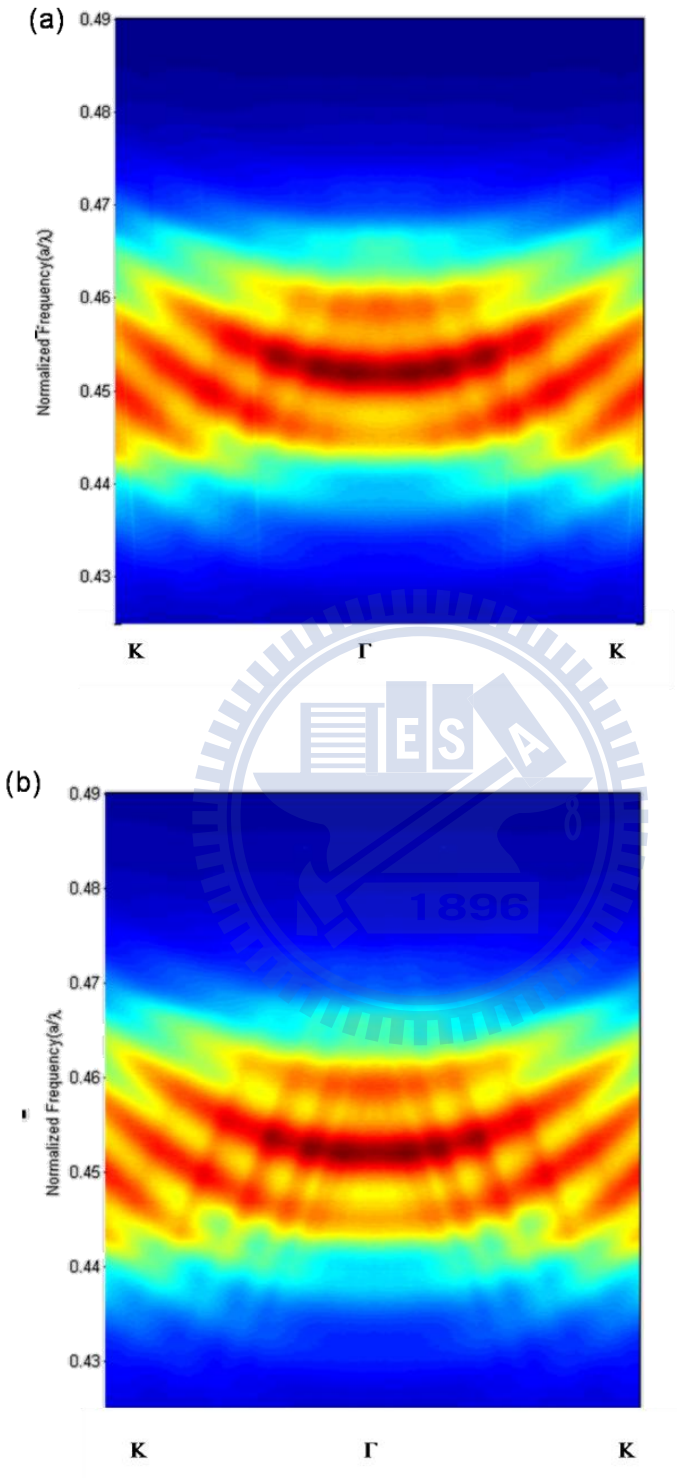
(a)
0.49
0.48
0.47
0.46
0.45
0.44
0.43
Normalized Frequency(a/λ)
K
Γ
K
(b)
0.49
0.48
0.47
0.46
0.45
0.44
0.43
Normalized Frequency(a/λ
K
Γ
K

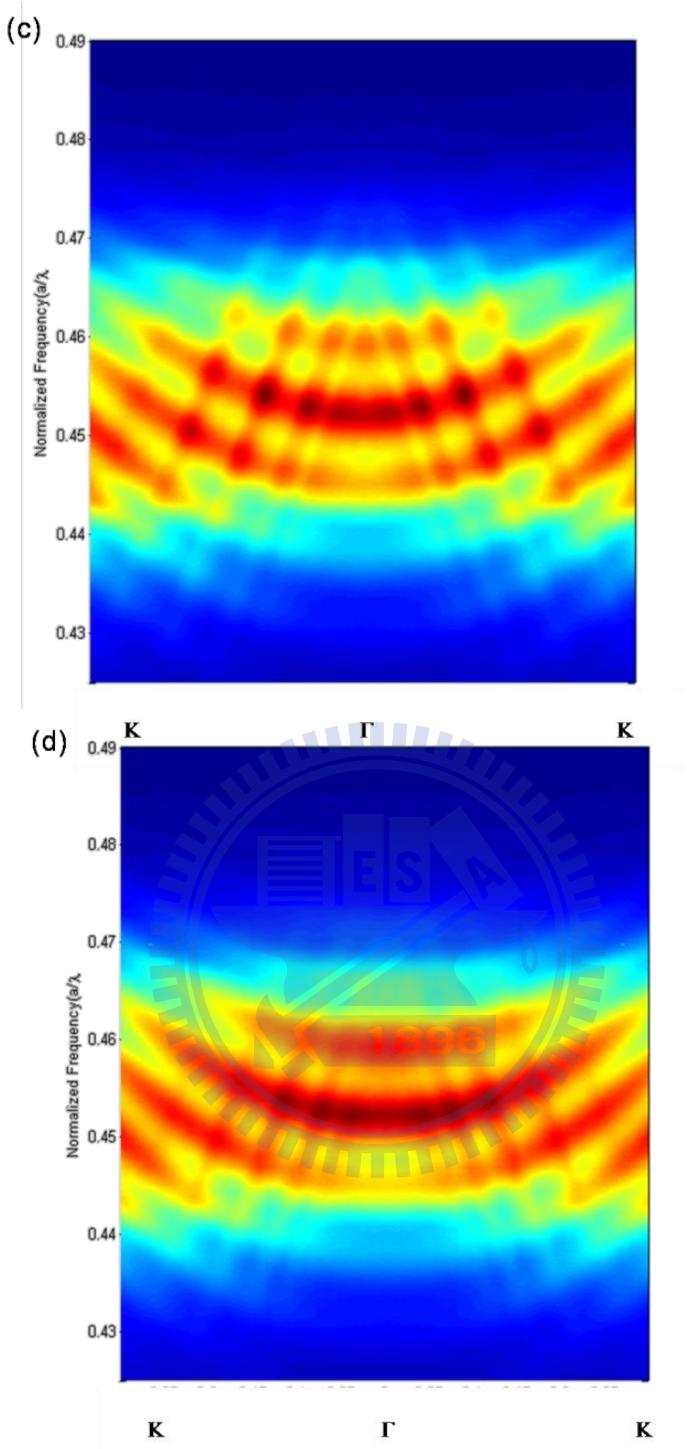

Figure 4-5 The angle-resolved μ-PL(a)H0 (b)H3 (c)H4 (d)H5 PCSELs diagram shows two kinds of modes : Fabry–Pérot modes (background broad curves), present in any planar structure with embedded QWs, and guided modes diffracted by the PhCs (sharp lines).

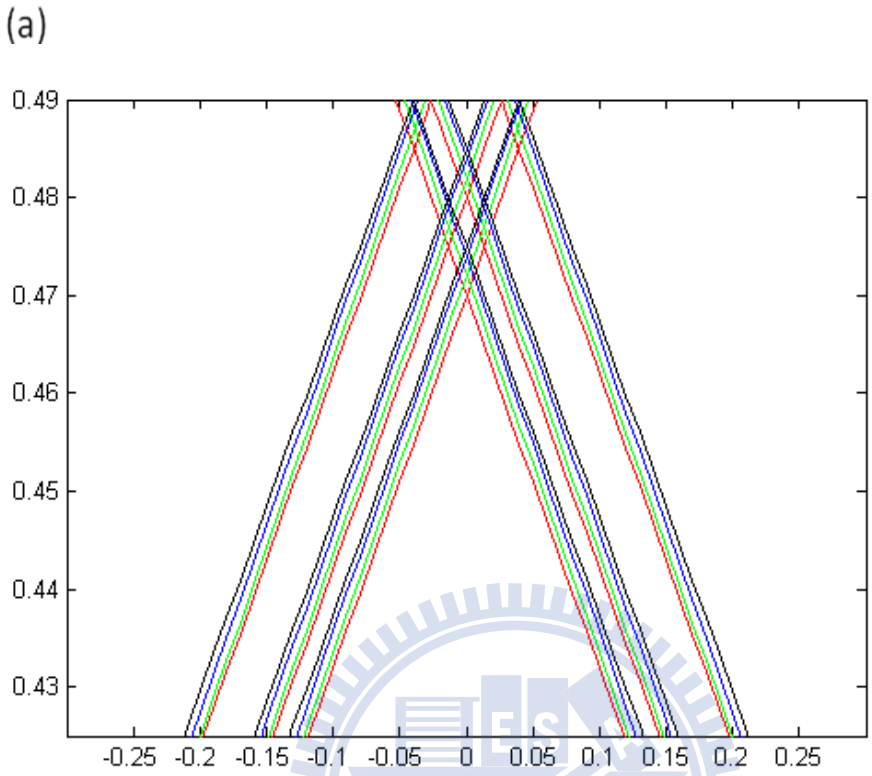

Figure 4-6 Band diagram fitting fromμ-PL

4-4 The lasing behavior of GaN-based 2D PCSELs with defects

Lasing wavelength

The PCSELs is fabricated by the standard process flowchart. The r/a ratio (where r is the radius of hole, a is lattice constant) of PhCs is 0.21. We optical pumped the PCSEL at 300K and the lasing spectrum is shown in Figure 4-7 4-8 4-9 and Figure 4-10. , lasing wavelength are about 400nm , 398nm 392nm and 390 nm respectively.

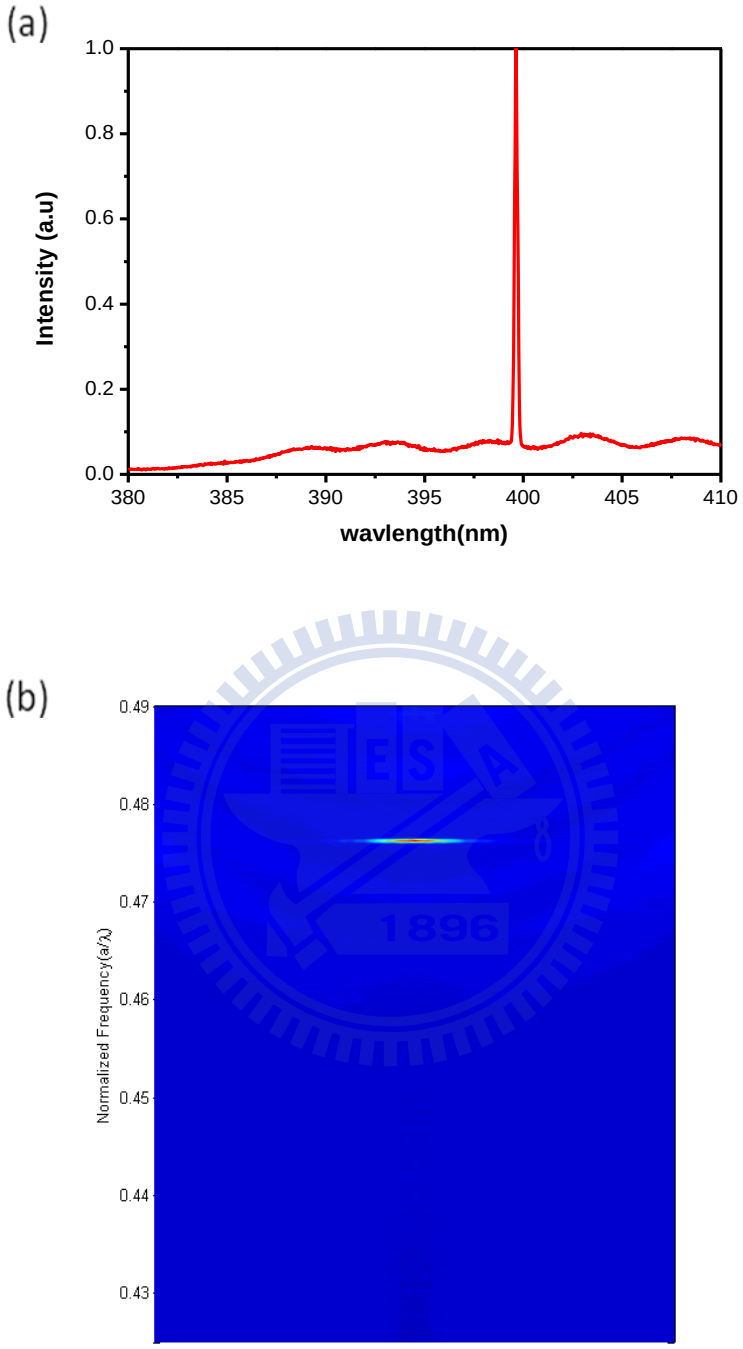

Figure 4-7 H0 PCSEL (a)lasing spectrum and (b)angle-resolved lasing spectrum

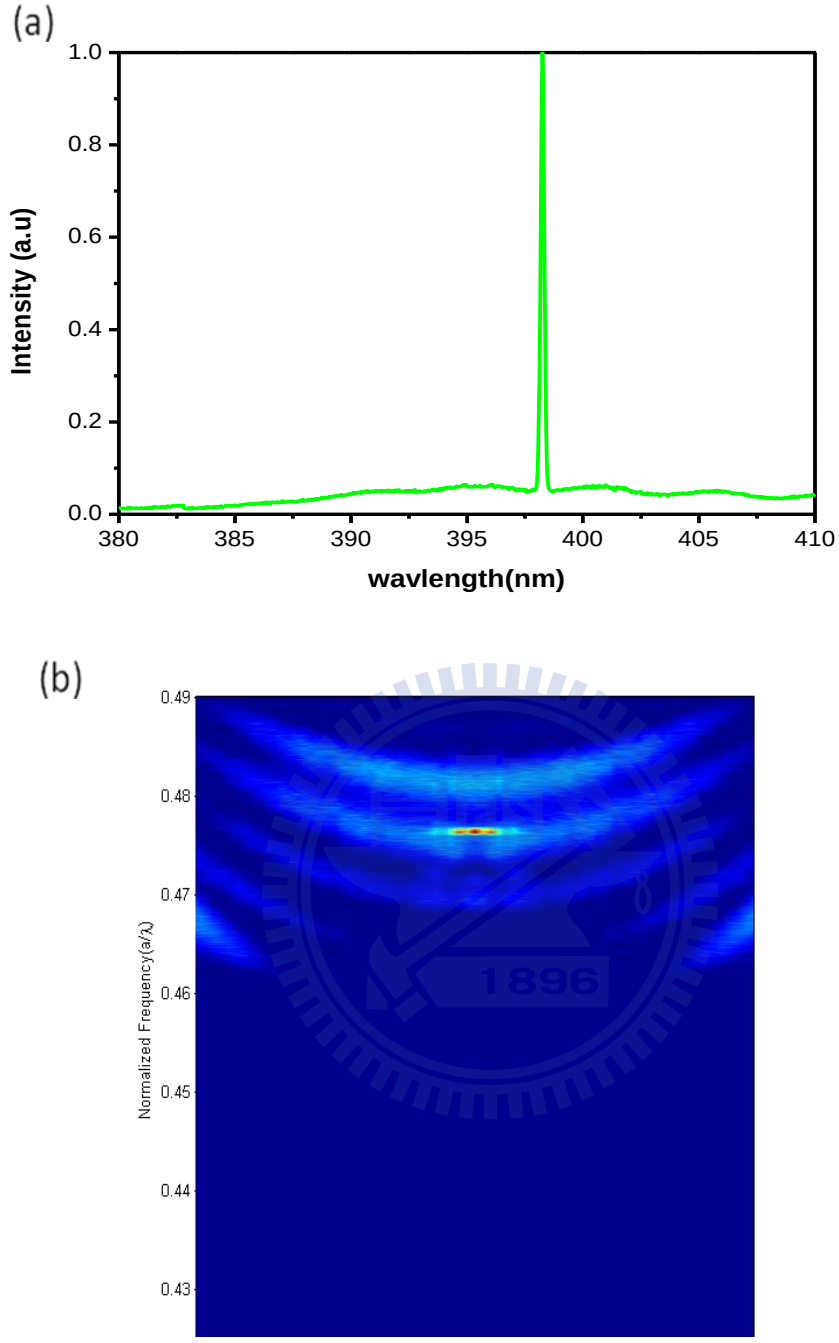

Figure 4-8 H3 PCSEL (a)lasing spectrum and (b)angle-resolved lasing spectrum

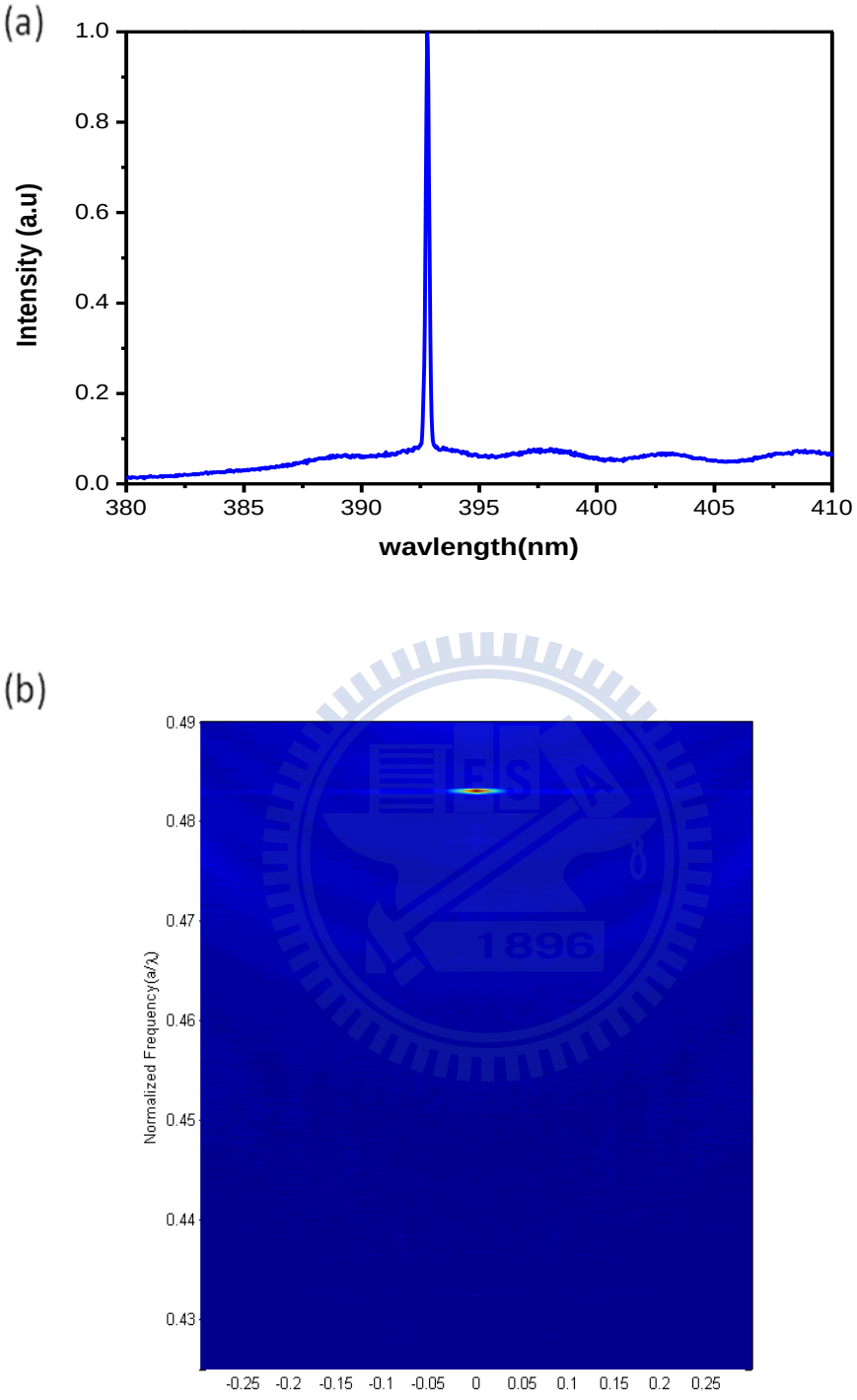

Figure 4-9 H4 PCSEL (a)lasing spectrum and (b)angle-resolved lasing spectrum

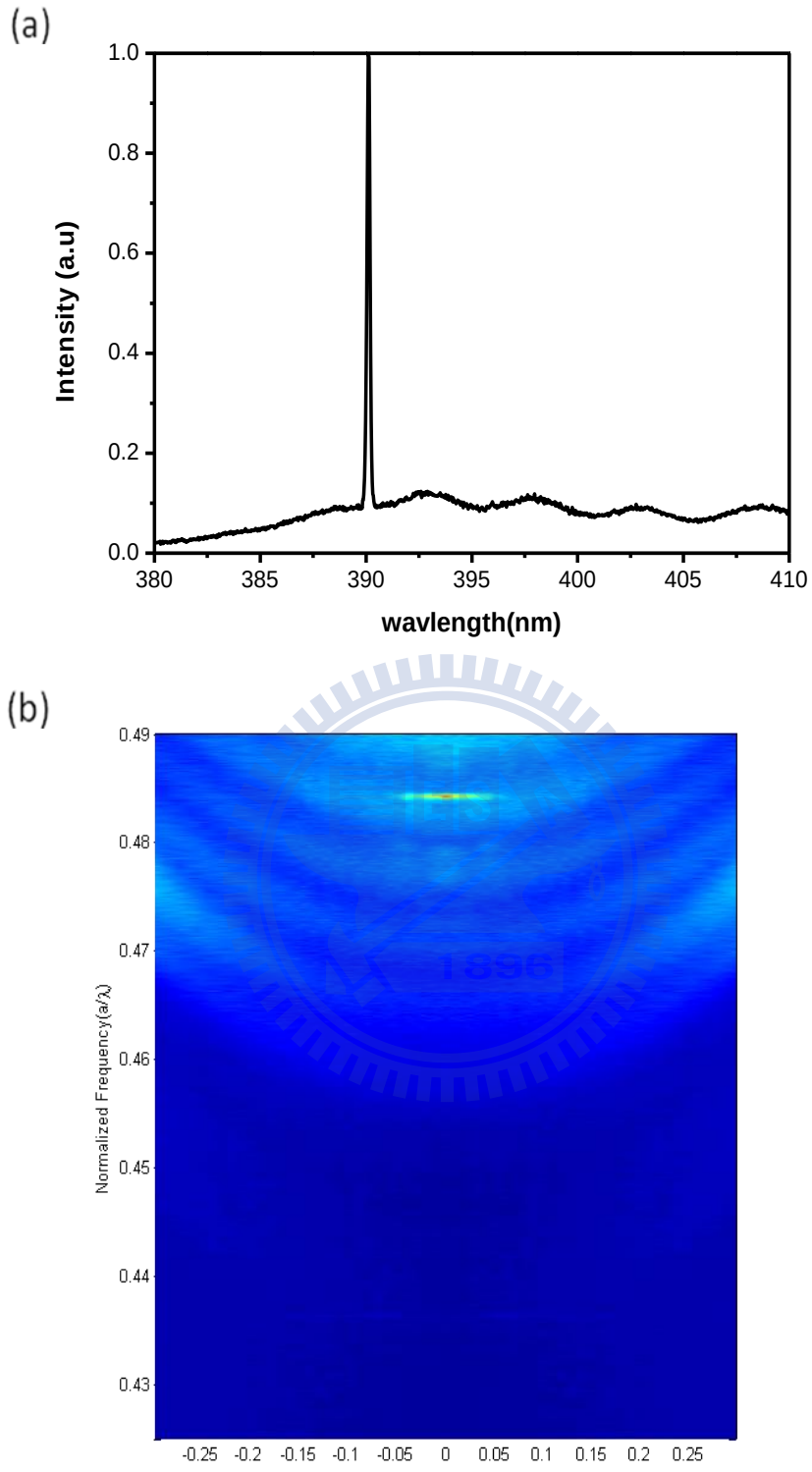

Figure 4-10 H5 PCSEL (a)lasing spectrum and (b)angle-resolved lasing spectrum

At first, we consider the effect of defects in photonic crystal. By the angle

resolved spectrum as shown in fgure4-5 ,and the fitting curves in figure 4-6,we can verify that lasing characteristic are similar for different defects in PCSEL.

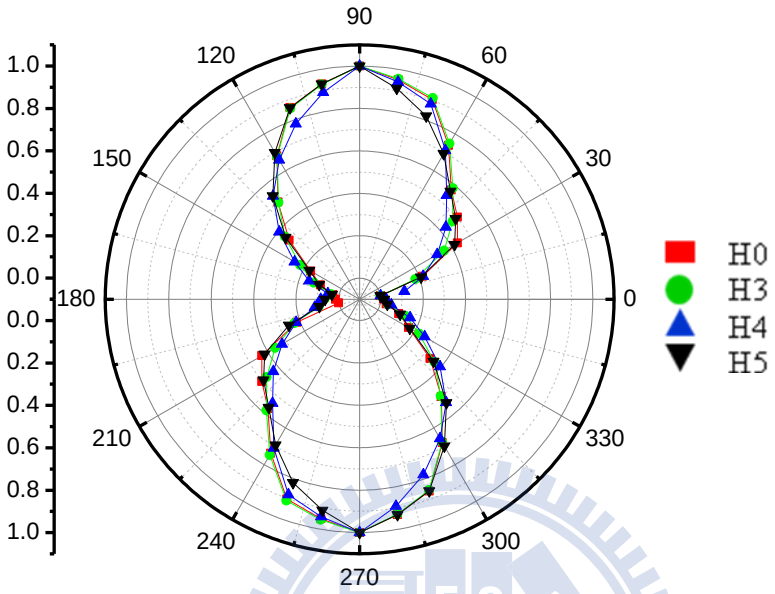

Figure 4-11 Polarization of H0 ,H3,H4 and H5underasing condition

Secondly, from the polarization characteristic as shown in figure4-11,we can judge their lasing feedback is at similar band-edge mode(Γ1).

Then we apply cavity model for 2D defects in photonic crystal as shown in figure 4-12.If we calculate the relation between reflection and detuning wavelength, we can find a stop band and band-edge in the spectrum .Considering the gain coefficient , we find that the lasing action arise from band-edge mode and cavity mode as shown in figure 4-13(a)(b).[2]

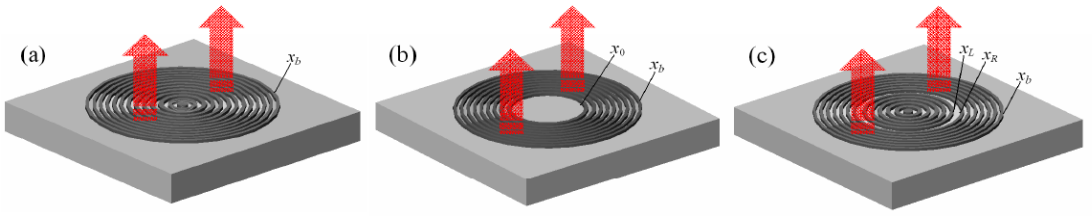

Figure 4-12 schematic of (a) circular DFB laser (b) disk Bragg resonator (c) ring Bragg resonator.

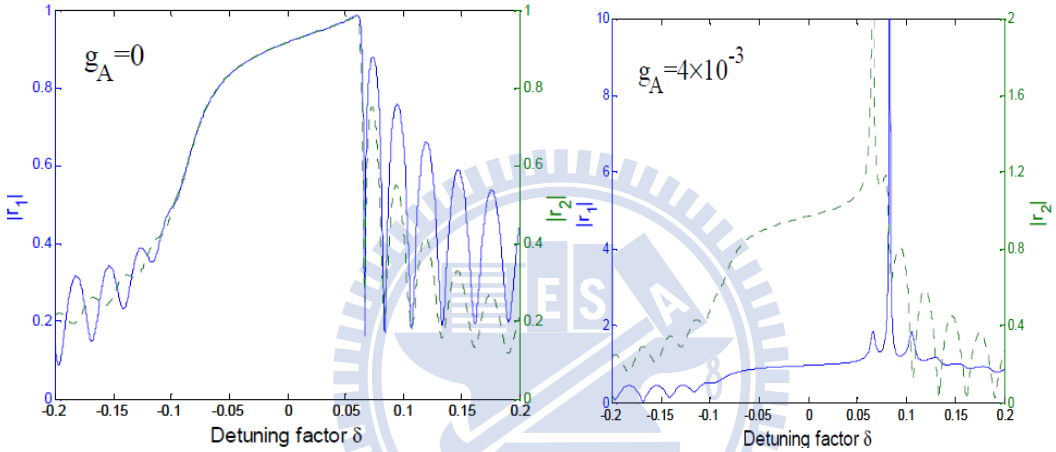

Figure4-13 simulation of reflection (a) without gain (b) with gain coefficient

Finally we calculate our PCSEL cavity mode to find lasing wavelength shifts in different defect types of PCSELs. Because our PCSEL period is about 190nm and radius is about 40nm. Its first stop band is located at 1200nm with FWHM about 24nm. And second stop band is located at 394nm with FWHM about 7.6nm. In our PCSELs structure, the lasing action arise from second order diffraction as shown in figure 4-15.

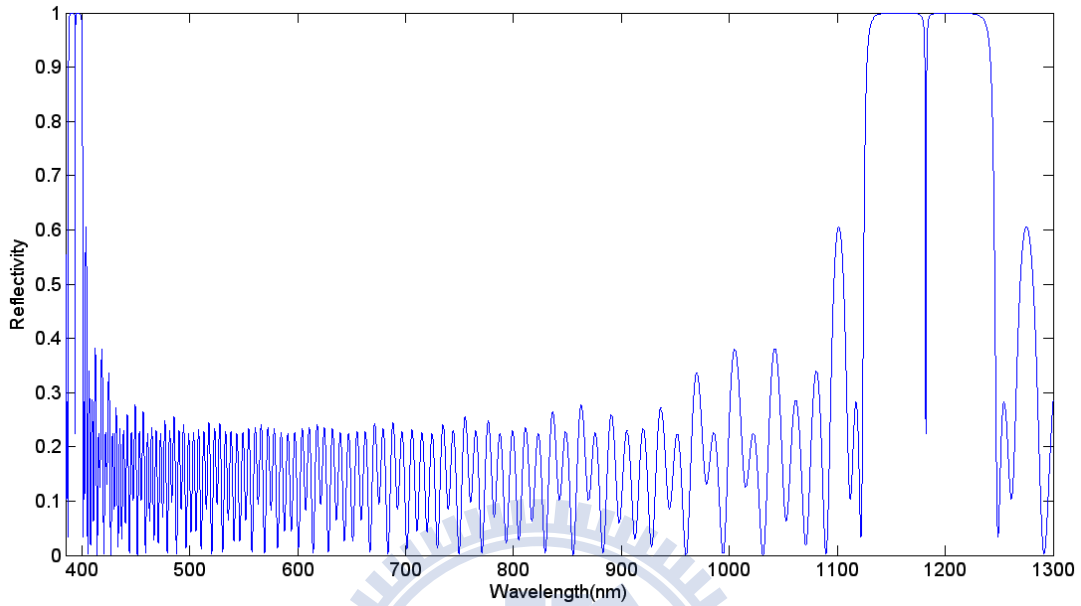

Fig4-14 Cavity mode simulation for our PCSELs structure (first order stop band)

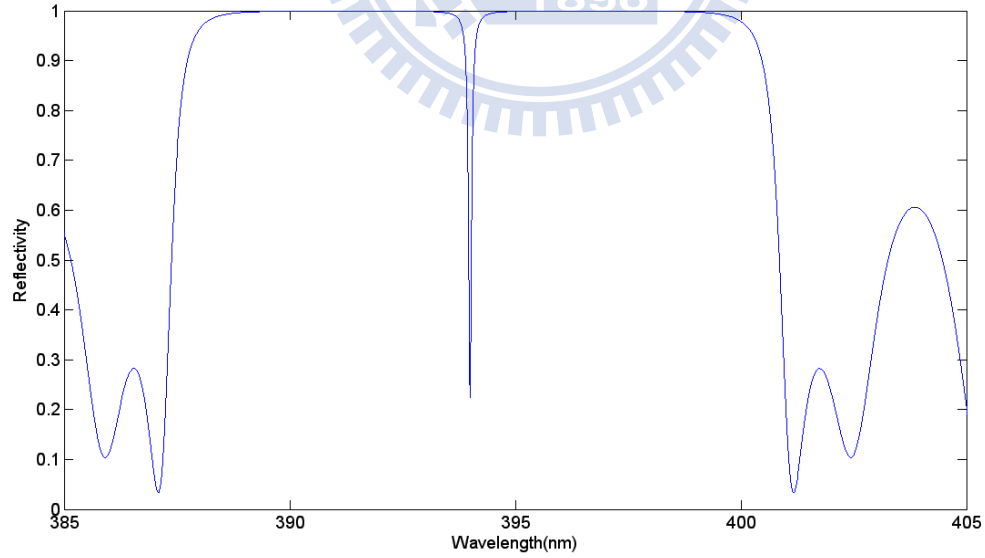

Fig4-15 Cavity mode simulation for our PCSELs structure (second order stop band)

If we take consideration of gain coefficient and different cavity length as different defect size, cavity mode arise and shifts with different cavity length. And cavity mode shifts per lambda divided by two .

As mentioned above, the difference between defects in PCSELs can be verified as second order diffraction and cavity mode detuning. We simulated the relation in our case to mapping the result as shown in figure 4-16. For H0, lasing wavelength is located at band-edge mode, which is 400nm. For H3 ,lasing wavelength is located at cavity mode , cavity length divided by normalized cavity length is about 12.37 , so we can map its lasing wavelength to 398nm . For H4 , lasing wavelength is located at cavity mode , cavity length divided by normalized cavity length is about 16.71 , so we can map its lasing wavelength to 392nm . For H5 , lasing wavelength is located at cavity mode , cavity length divided by normalized cavity length is about 20.7 , so we can map its lasing wavelength to 390nm

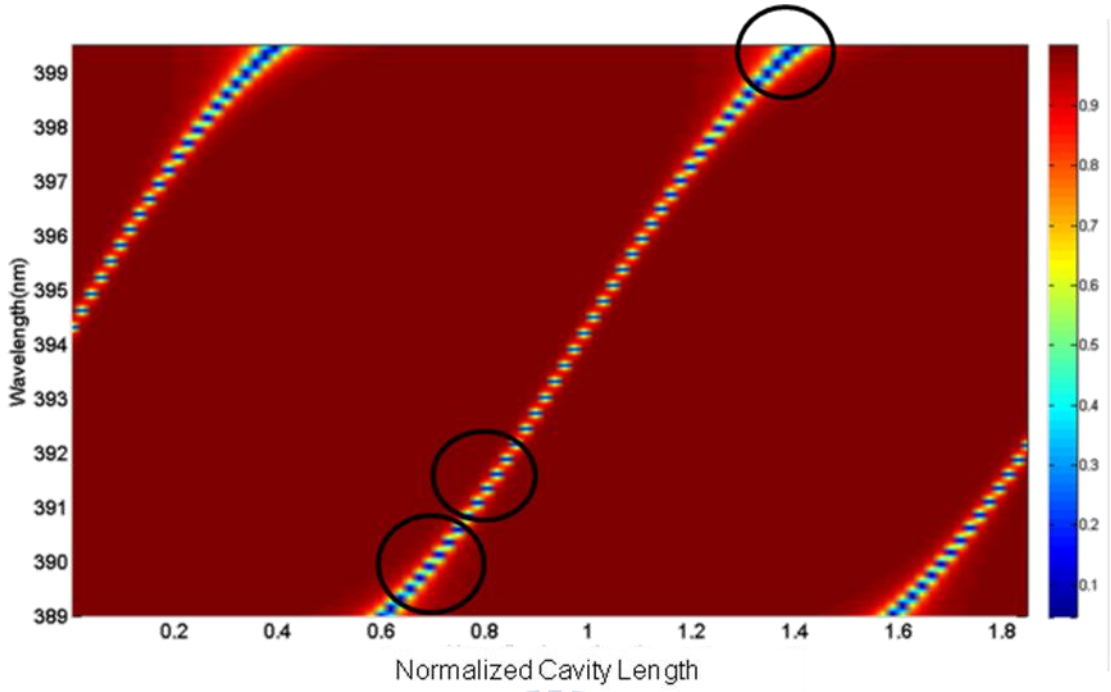

Fig4-16 Mapping diagram of relation between cavity mode and cavity length.

Defect	Lasing wavelength	Normalized Frequency	Cavity length(nm)	Normalized Cavity length
H0	400	0.475		
H3	398	0.477	977	12.37
H4	392	0.485	1320	16.71
H5	390	0.487	1635	20.7

Table4-1 The parameter of different defects of PCSELs

Lasing Threshold

PCSELs are based on the reflection and feedback on periodical change in air rod. If there exist localized defects in PCSELs and the lasing action is not localized in the defect. Because of the reduction of reflection and cavity mode shifts, threshold value increases by the lack of reflection as in our PCSELs.Fig4-17.There should be further confirmed by couple wave simulation method.

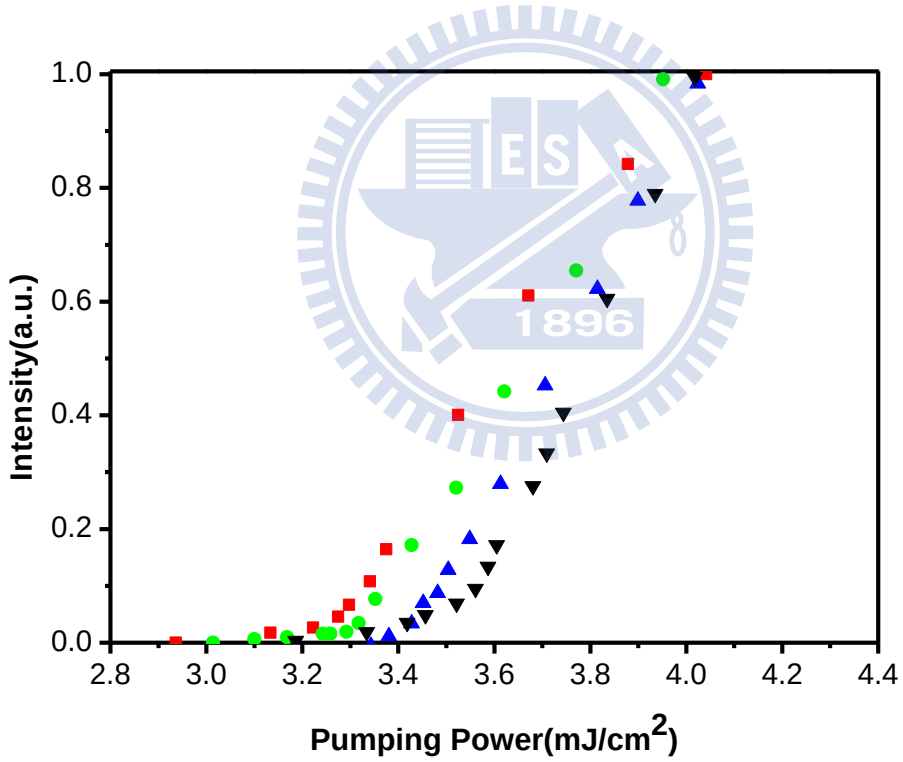

Fig4-17 Lasing threshold and table for H0 ,H3 ,H4 and H5

Reference

[1] Fre´de´ric S. Diana, Aure´lien David, Ines Meinel, Rajat Sharma, Claude Weisbuch, Shuji Nakamura, and Pierre M. Petroff, *Nano Lett.* **6**, 1116-1120 (2006)

[2]Xiankai sun and Amnon Yariv *OPTICS EXPRESS* **16**, 9155(2008)

[3] Antonio Badolato, Kevin Hennessy, Mete Atatu¨re,Jan Dreiser,3 Evelyn Hu,Pierre M. Petroff, Atac Imamog˘lu *Science* **308** , 1158 (2005)

Chapter 5

Conclusion

In this thesis, we investigated the optical characteristics and the effect of defects in GaN-based 2D photonic crystal surface emitting lasers (PCSELs). According to the theory, the lasing behavior in the photonic crystal grating structure could only happen as the Bragg condition is satisfied. Therefore, the lattice constant is determined to be 190 nm considering PL peak centered at a wavelength of 400nm.

The lasing wavelength varies from 390nm to 400nm for different defects. For the device without defect , lasing wavelength is located at 400nm and blue shift to 390 nm with largest defect(H5).We use plane wave expansion method (PWEM) to simulate the TE band diagram. Normalized frequency of investigated PC lasing wavelength can correspond to band-edge frequency (Γ1), which indicates the lasing action can only occur at specific band-edge. Polarization states further confirm the existence of lasing modes at band-edge (Γ1).

By the angle-resolved micro-photoluminescence measurement, we find out that the band structure are similar for different defects photonic crystal surface emitting laser.

To understand the trend of wavelengths variation in different defect devices, we take the 1D DFB laser as our simulation model. Because the lattice constant is 190 nm and radius is about 40~50nm , the first-order stop band is located about 1200 nm , and the second-order stop band is located about 395 nm . From the calculation result, the diffraction and cavity mode arise from the second-order stop band.

We apply the cavity mode detuning theory, cavity mode shifts with cavity length , and calculate cavity mode detuning which indicates H3 corresponding to 398nm , H4 corresponding to 390 nm and H5 corresponding to 390nm.Besides,Lasing threshold

power increasing with larger defect size is the result of coupling and feedback strength decreasing with photonic crystal.